

This is the accepted manuscript made available via CHORUS. The article has been published as:

Giant magnetoelectric effect in pure manganite-manganite heterostructures

Sanjukta Paul, Ravindra Pankaj, Sudhakar Yarlagadda, Pinaki Majumdar, and Peter B. Littlewood

Phys. Rev. B **96**, 195130 — Published 14 November 2017

DOI: [10.1103/PhysRevB.96.195130](https://doi.org/10.1103/PhysRevB.96.195130)

Giant magnetoelectric effect in pure manganite-manganite heterostructures

Sanjukta Paul¹, Ravindra Pankaj¹, Sudhakar Yarlagadda¹, Pinaki Majumdar², and Peter B. Littlewood^{3,4}

¹*CMP Div., Saha Institute of Nuclear Physics, HBNI, Kolkata, India*

²*Harish-Chandra Research Institute, HBNI, Allahabad, India*

³*Argonne National Laboratory, Argonne IL 60439 and*

⁴*University of Chicago, James Franck Institute, Chicago IL 60637*

(Dated: September 22, 2017)

Obtaining strong magnetoelectric couplings in bulk materials and heterostructures is an ongoing challenge. We demonstrate that manganite heterostructures of the form (Insulator)/(LaMnO₃)_n/Interface/(CaMnO₃)_n/(Insulator) show strong multiferroicity in magnetic manganites where ferroelectric polarization is realized by charges leaking from LaMnO₃ to CaMnO₃ due to repulsion. Here, an effective nearest-neighbor electron-electron (electron-hole) repulsion (attraction) is generated by cooperative electron-phonon interaction. Double exchange, when a particle virtually hops to its unoccupied neighboring site and back, produces magnetic polarons that polarize antiferromagnetic regions. Thus a striking giant magnetoelectric effect ensues when an external electrical field enhances the electron leakage across the interface.

PACS numbers: 75.85.+t, 71.38.-k, 71.45.Lr, 71.38.Ht, 75.47.Lx, 75.10.-b

I. INTRODUCTION

Complex oxides such as manganites display a rich interplay of various orbital, charge, and spin orders when rare-earth dopants are added to the parent oxide. While significant progress has been made in characterizing the bulk doped materials, the heterostructures produced from two parent oxides is an area of active research^{1,2}. In these heterostructures, the accompanying quantum confinement, anisotropy, heterogeneity, and the enhanced gradients (in magnetic moments, electric potential, orbital polarization, etc.) across the interface result in novel phenomena that have no counter part in the bulk samples^{3,4}. In fact, the challenge is to technologically exploit this new physics and develop new useful devices that can meet future demands such as miniaturization, dissipationless operation/manipulation (such as read/write capability), energy storage, etc⁵⁻¹¹.

There has been a revival in multiferroic research partly due to improved technology, discovery of new compounds (such as YMnO₃, TbMn₂O₅), need for devices with strong magnetoelectric effect, etc¹². Majority of the multiferroics studied are bulk materials where it is not yet clear why the magnetic and electric polarizations coexist poorly¹³. With the advent of improved molecular-beam-epitaxy technology one can now grow oxide heterostructures with atomic-layer precision and explore the possibility of strong multiferroic phenomena as well as large interplay between ferroelectricity and magnetic polarization. Coupling between the charge and spin degrees of freedom is fascinating both from a fundamental viewpoint as well as from an applied perspective. Instead of employing currents and magnetic fields, controlling and manipulating magnetism with electric fields holds a lot of promise as the electric fields are easier to use in smaller dimensions and can potentially lower energy consumption in systems. There are numerous mechanisms for magnetoelectric effect; reviews for these can be found in

Refs. 14–18. At the interface of a magnetic oxide and a ferroelectric/dielectric oxide, magnetoelectric effect of electronic origin has been predicted by some researchers. Upon application of an external electric field, not only the magnitude of moments can be changed^{19,20}, but in some cases the very nature of magnetic ordering can be changed²¹.

Among various efforts pertaining to oxide heterostructures, there is considerable interest, both experimentally²²⁻²⁹ as well as theoretically³⁰⁻³⁵, in understanding novel aspects of conductivity, magnetism, and orbital order in pure manganite-manganite TMnO₃/DMnO₃ heterostructures where T refers to trivalent rare earth elements La, Pr, Nd, etc. and D refers to divalent alkaline elements Sr, Ca, etc. At low temperatures, the bulk TMnO₃ is an insulating A-type antiferromagnet (A-AFM); on the other hand, the bulk DMnO₃ is an insulating G-type antiferromagnet (G-AFM). Furthermore, the doped alloy T_{1-x}D_xMnO₃ is an antiferromagnet for $x > 0.5$; whereas for $x < 0.5$, it is a ferromagnetic insulator (FMI) at smaller values of x (i.e., $0.1 \lesssim x \lesssim 0.2$)³⁶⁻³⁸ and is a ferromagnetic metal at higher dopings in La_{1-x}Sr_xMnO₃, La_{1-x}Ca_xMnO₃, Pr_{1-x}Sr_xMnO₃, and Nd_{1-x}Sr_xMnO₃. For representative studies of doped manganite-manganite heterostructures, the reader is referred to Ref. 39.

In spite of considerable efforts towards control of magnetization through electric fields in multiferroic bulk materials and heterostructures, obtaining strong magnetoelectric couplings continues to be a challenge. Here, in this paper, we predict a novel giant magnetoelectric effect, not at the interface, but away from it, in a pure manganite-manganite heterostructure (see Fig. 1). We present a plausible multiferroic phenomenon in manganite heterostructures and point out the associated unnoticed striking magnetoelectric effect. Cooperative electron-phonon interaction is shown to be key to understanding both multiferroicity and magnetoelectric effect

in our oxide heterostructure. Here, we exploit the fact that manganites have various competing phases that are close in energy and that by using an external perturbation (such as an electric or a magnetic field) the system can be induced to alter its phase. We show that there is a charge redistribution (with a net electric dipole moment perpendicular to the interface) due to the optimization produced by the following two competing effects: (i) energy cost to produce holes on the LaMnO_3 (LMO) side and excess electrons on the CaMnO_3 (CMO) side; and (ii) energy gain due to electron-hole attraction (or electron-electron repulsion) on nearest-neighbor Mn sites induced by electron-phonon interaction. The charge polarization is akin to that of a pn-junction in semiconductors although the governing equations are different. The minority carriers, which leak across the interface of the heterostructure, produce ferromagnetic domains due to the ferromagnetic coupling (generated by electron-phonon interaction and double-exchange) between an electron-hole pair on adjacent sites. Since ferroelectricity and ferromagnetism have a common origin [i.e., minority carriers or holes (electrons) on LMO (CMO) side], there is a striking interplay between these two polarizations; consequently, when an external electric field is applied to increase the minority carriers, a giant magnetoelectric effect results.

We will argue that a large magnetoelectric effect is possible in LMO-CMO heterostructures by presenting below cohesive general theoretical points which take into account the essential features of manganites without invoking any particular model.

1) Kinetic energy (KE) is quite small because bare hopping is small (caused by lower tolerance factor⁴⁰, cation disorder, and compatibility of distortions⁴¹), electron-phonon coupling is strong, and system is quasi-two-dimensional (q2D).

2) Potential energy [from Coulomb interaction and nearest-neighbor (NN) particle-particle repulsion due to cooperative electron-phonon interaction] is much larger than KE; this leads to solid-type formation with electrons being rendered essentially immobile. Then, in each layer parallel to the interface (see Fig. 1), a solid with close-to-crystalline symmetry is formed with electrons being essentially site localized. The ground state is classical with number density at each site either 1 or 0 and the state of the system can be expressed by a single state in the occupation number basis. Due to strong cooperative electron-phonon interaction (CEPI) and not due to a sizeable KE, there is a propensity for electrons to migrate from the LMO side to the CMO side; this leads to a density gradient in the direction perpendicular to the interface (z-direction).

The fact that electrons are essentially site localized also follows when the treatment in Ref. 42 is extended to our q2D system; then, only a localized polaronic band is relevant and the upper wide band cannot overlap with the lower narrow polaronic band. Additionally, the insulating behavior reported in Ref. 22 for

$(\text{LaMnO}_3)_{2n}/(\text{SrMnO}_3)_n$ superlattice (when $n > 2$) further justifies the picture of negligible KE with the potential energy determining the charge and spin order.

3) Because of Coulomb interaction between charges and strong CEPI, checkerboard-type crystal occurs in layers with densities close to 0.5 (based on point 2); checkerboard arrangement (including in the z-direction) is expected in layers next to the interface since there the density is 0.5 due to symmetry considerations. This checkerboard feature is different from bulk manganites where charge and orbital stacking in z-direction occurs [and leads to the CE-type antiferromagnet (CE-AFM)]; this type of charge order was missed in works such as Ref. 34 because CEPI was not considered. Strong electron-phonon interaction produces NN electron-hole pair and produces between the pair a strong ferromagnetic interaction [$t^2 \cos^2(\theta/2)/E_{\text{JT}}$ with E_{JT} being the cooperative Jahn-Teller energy, t the hopping term between the NN sites, and θ the angle between the core spins of the NN sites]. Hence, a ferromagnetic state is produced in the checkerboard. CE-type spin order is not supported because charge does not stack up in the z-direction; consequently, zigzag ferromagnetic chains in adjacent layers of the checkerboard will not be formed as such chains cannot be stacked up to produce between them magnetic coupling (such as antiferromagnetic) which is essential to the CE-type magnetism.

4) The model for magnetic interaction pertains to LMO-CMO heterostructure with localized holes. The CEPI retains essentially the same orbital texture as in LMO in regions away from the holes. Consequently, on the LMO side, the magnetic interaction is A-AFM in regions without holes; this interaction is generated through virtual hopping by localized electrons between NN sites that are Jahn-Teller compatible. When holes are present, since they are site localized, they only virtually hop to NN site and back and produce ferromagnetic coupling with NN electrons; this coupling is much stronger than A-AFM coupling. To go beyond the above picture (as was done rigorously in Ref. 43 for LaMnO_3), involves the daunting task of taking into account coupling between t_{2g} spins [$J_{t_{2g}}$], two-band model, Hubbard U , long-range Coulomb interaction, realistic Hund's coupling J_H ($< U$), and cooperative Jahn-Teller energy E_{JT} in a sizeable system (i.e., a lattice with about 100 sites or more) with LMO side being at finite hole density. We are not aware of such a comprehensive approach being reported.

5) Presence of site localized holes on the LMO side, produces FMI clusters due to formation of magnetic polarons. A hole will polarize nearest-neighbor electrons (and realistically speaking, next-nearest-neighbor and next-to-next-nearest-neighbor electrons as well) through virtual hopping, thereby producing a magnetic polaron. A collection of interacting magnetic polarons will produce a FMI region. This picture is in tune with FMI region being a generic feature of manganites at moderate dopings ($0.1 \lesssim x \lesssim 0.2$); see Ref. 42 for a similar FMI picture in the bulk. It should be noted that FMI re-

gions are present in moderately-doped manganites that are narrow band ($\text{Pr}_{1-x}\text{Ca}_x\text{MnO}_3$), intermediate band ($\text{La}_{1-x}\text{Ca}_x\text{MnO}_3$) and wide band ($\text{La}_{1-x}\text{Sr}_x\text{MnO}_3$). Increasing the number of holes on the LMO side, using a fairly large electric field, increases the number of aligned FMI clusters, thereby producing a large magnetoelectric effect. It is important to note that the applied electric field changes the magnetization sizeably in the bulk of LMO away from the interface while leaving the polarization at the interface essentially unaltered. Here, it should be noted that the FMI phase, which is key to the magnetoelectric effect, is not captured in the phase diagram of the bulk LCMO reported in Fig. 2 of Ref. 34; this is possibly because small values of $\lambda = \sqrt{2E_{JT}}/t$ were chosen and cooperativity in the electron-phonon interaction was ignored.

The rest of the paper is organized as follows. In Sec. II we introduce our phenomenological Hamiltonian (based on cooperative electron-phonon-interaction physics) using which we deduce the charge distribution in the continuum approximation. We also provide a simple analytic treatment for the magnetic profile and demonstrate a giant magnetoelectric effect in a few-layered heterostructure. Next, in Sec. III, we adopt a more detailed numerical approach and introduce a Hamiltonian that includes additional kinetic terms, work functions, and discrete lattice effects. Here, magnetoelectric effect is studied in symmetric lattices (involving equal number of LMO and CMO layers) as well as in asymmetric lattices using Monte Carlo simulations. We close in Sec. IV with our concluding observations.

II. ANALYTIC TREATMENT

We will begin our treatment of the pure manganite-manganite heterostructure by considering a simple analytic picture in this section and leave a more detailed numerical approach to the next section. Our (Insulator)/(LaMnO_3)_n/Interface/(CaMnO_3)_n/(Insulator) heterostructure is depicted in Fig. 1; the treatment in this section involves odd number of MnO_2 planes. The MnO_2 plane, contained in the Interface at the center, has LaO on one side and CaO on the other side. The MnO_2 plane in the center has 0.5 electron per Mn site. The arrangement of the heterostructure is as follows: Ins./(LaO-MnO_2)_n/($\text{LaO-MnO}_2\text{-CaO}$)/($\text{MnO}_2\text{-CaO}$)_n/Ins. where ($\text{LaO-MnO}_2\text{-CaO}$) represents the Interface. The above arrangement will not lead to polar catastrophe as any excess charge at the Ins./LaO interface can be neutralized by a gate potential. Alternately, the Ins./LaO interface on the left-hand side can be replaced by Ins./($\text{La}_{1/2}\text{Ca}_{1/2}\text{O}$) interface; then, no excess charge results.

A. Polaronic Hamiltonian

In our heterostructure depicted in Fig. 1, due to charge leaking across the LMO-CMO interface, we expect different states of the phase diagram of $\text{La}_{1-x}\text{Ca}_x\text{MnO}_3$ (LCMO) at different cross-sections perpendicular to the growth direction. Since far from the LMO-CMO interface the material properties must be similar to those in the bulk, we expect the $x = 0$ phase at the Insulator-LMO interface and the $x = 1$ phase at the other end involving CMO-Insulator interface. Considering majority of the LCMO phase diagram (including the end regions near $x = 0$ and $x = 1$) is taken up by insulating phases, since band width is significantly diminished at strong electron-phonon coupling, and because the heterostructures are q2D, we expect that there is no effective transport in the direction normal to the oxide-oxide interface (i.e., the z -direction). Then, for analyzing the charge distribution normal to the interface, the starting polaronic Hamiltonian is assumed to comprise of localized electrons and have the following phenomenological form:

$$H_{\text{pol}} \sim - \sum_{j,\delta} \left[\gamma_{\text{ep}}^1 g^2 \omega_0 + \frac{\gamma_{\text{ep}}^2 t_{j,j+\delta}^2}{g^2 \omega_0} \right] n_j (1 - n_{j+\delta}), \quad (1)$$

where the first coefficient $\gamma_{\text{ep}}^1 g^2 \omega_0$ is due to electron-phonon interaction and represents nearest-neighbor electron-electron repulsion brought about by incompatible distortions of nearest-neighbor oxygen cages surrounding occupied Mn ions. The pre-factor γ_{ep}^1 can depend on the phase – for instance, in the regime of C-type antiferromagnet (C-AFM) in LCMO, γ_{ep}^1 is expected to be large because occupancy of neighboring d_{z^2} orbitals is inhibited in the z -direction; while in the regime of A-AFM (corresponding to undoped LaMnO_3), γ_{ep}^1 is expected to be weaker because of compatible Jahn-Teller distortions on neighboring sites. Here, we will assume for simplicity that γ_{ep}^1 is concentration independent and that $0.1 \leq \gamma_{\text{ep}}^1 \leq 1$. Next, the coefficient $\gamma_{\text{ep}}^2 t^2 / (g^2 \omega_0)$ results from processes involving hopping to nearest-neighbor and back and is present even when we consider the simpler Holstein model⁴⁴ or the Hubbard-Holstein model⁴⁵. The pre-factor γ_{ep}^2 varies between 1/2 (for non-cooperative electron-phonon interaction) and 1/4 (since for cooperative breathing mode in one-dimensional chains $\gamma_{\text{ep}}^2 = 1/3$, which should be more than in C-chains)⁴⁶. Now, even within the two-band picture of manganites in Ref. 42, the electrons in the localized polaronic band contribute the term $t^2 / g^2 \omega_0$; the broad band (due to undistorted states that are orthogonal to the polaronic states) is an upper band whose band width is reduced due to the two-dimensional (2D) nature of the system and does not overlap with the polaronic band to produce conduction even at carrier concentrations corresponding to $0.2 \lesssim x \lesssim 0.5$. Furthermore, although n_j is the total number in both the orbitals at site j , it can only take a maximum value of 1 due to strong on-site electron-electron repulsion and strong Hund's coupling. Next, to make the above Hamil-

tonian furthermore relevant for manganites, one needs to consider Hund's coupling between core t_{2g} spins and itinerant e_g electrons. This leads to invoking the double exchange mechanism for transport. Then, the hopping term $t_{i,j}$ between sites i and j in Eq. (1) is modified to be $t_{i,j}\sqrt{0.5[1+(\mathbf{S}_i \cdot \mathbf{S}_j/S^2)]} = t_{i,j}\cos(\theta_{ij}/2)$ with \mathbf{S}_i being the core t_{2g} spin at site i and θ_{ij} being the angle between \mathbf{S}_i and \mathbf{S}_j . The term $\gamma_{ep}^2 t_{j,j+\delta}^2 \cos^2(\theta_{ij}/2)/(g^2\omega_0)$ in Eq. (1) produces a strong ferromagnetic coupling between the spins at site j and site $j+\delta$ and this dominates over any superexchange coupling between the two spins.

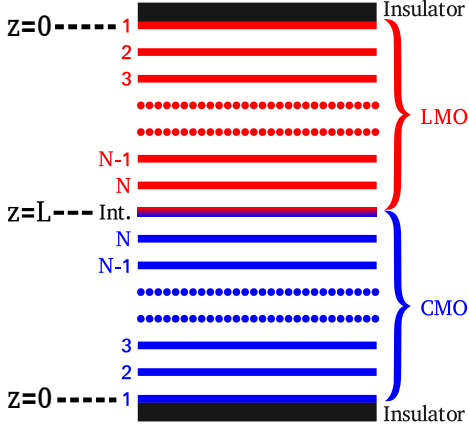


FIG. 1. (Color online) Schematic showing the symmetric (Insulator)/(LaMnO₃)_N/Interface/(CaMnO₃)_N/(Insulator) heterostructure. Each of the labeled N layers on both LMO (LaMnO₃) and CMO (CaMnO₃) sides contain manganese-oxide (MO) layers.

B. Charge Profile

The kinetic term is small due to polaronic effects and the q2D nature of the system. While the complete absence of kinetic energy would indeed lead to the electron charge density following the ionic charge, in the presence of a small kinetic term the charge profile will redistribute. We just assume that the kinetic contribution to the energy is small compared to the other terms, not that the charges are fully immobilized.

The following are two competing terms in the potential energy which are the dominant terms that produce charge distribution:

- 1) Due to cooperative electron-phonon interactions, there is a repulsive interaction between electrons on adjacent sites. This pushes electrons from LMO side to CMO side.
- 2) There is attractive interaction between an electron on a Mn site and the positive ionic charge of that unit cell. This attraction holds back the electrons on the LMO side.

Now, when the electrons move from the LMO side to the CMO side, there is a net positive charge on the LMO side and a net negative charge on the CMO side. The

separation energy of these net positive and net negative charges can be approximated as the energy of a capacitor $Q^2/2C_{\text{cap}}$ where charge $Q \sim N_{\text{el}}$ (with N_{el} being the transferred electrons) and capacitance $C_{\text{cap}} \propto A_{\text{int}}/d$ with A_{int} being the interface area and d the separation; this energy (i.e., $Q^2/2C_{\text{cap}}$) has to be balanced by the nearest-neighbor repulsion energy ($\sim N_{\text{el}}g^2\omega_0$) due to electron-phonon interaction. Now, if Q/A_{int} is independent of the system size and d is only a few lattice spacings, then $Q^2/2C_{\text{cap}}$ can be comparable to $\sim N_{\text{el}}g^2\omega_0$; thus, macroscopic number of charges, from a few layers near the interface, can be transferred across the interface. Hence, ideally the heterostructure should comprise of only a few layers so that a large part of the system can contribute to the multiferroicity and also the magneto-electric effect.

To obtain the charge distribution, we ignore the effect of superexchange interaction in the starting effective Hamiltonian in Eq. (1) because its energy scale is significantly smaller than the polaronic energy term $2g^2\omega_0$. For a localized system, we only need to minimize the interaction energy which is a functional of the electronic density profile. The Coulombic interaction energy resulting from the electrons leaking from the LMO side to the CMO side, is taken into account by ascribing an effective charge $+1$ (hole) to the LMO unit cell (centered at the Mn site) that has donated an e_g electron from the Mn site and an effective charge -1 (electron) to the CMO unit cell (centered at the Mn site) that has accepted an e_g electron at the Mn site. The Coulombic energy that results is due to the interactions between these ± 1 effective charges. The net positive charge on the LMO side and the net negative charge on the CMO side will produce a charge polarization (or inversion asymmetry). Since the ferroelectric dipole is expected to be in the direction perpendicular to the oxide-oxide (LMO-CMO) interface, we assume that the density is uniform in each layer for calculating the density profile as a function of distance z from the insulator-oxide interface. The Coulombic interaction energy per unit area due to leaked charges is the same for both LMO and CMO regions and is given, in the continuum approximation, to be

$$E_{\text{coul}} = \frac{1}{8\pi\epsilon} \int_0^L dz D(z)^2, \quad (2)$$

where $D(z)$ is the electric displacement and is given by

$$D(z) = \pm \left[-\epsilon E_{\text{ext}} + \int_0^z dy 4\pi e \rho(y) \right], \quad (3)$$

with $+$ ($-$) sign for LMO (CMO) side. Furthermore, $\rho(z)$ is the density of minority charges (i.e., holes on LMO side and electrons on SMO side), e the charge of a hole, ϵ the dielectric constant, E_{ext} an external electric field along the z -direction, and L the thickness of the LMO (CMO) layers.

The ground state energy per unit area [corresponding to the effective Hamiltonian of Eq. (1)] can be written,

in the continuum approximation, as a functional of $\rho(z)$ for both LMO and CMO as follows:

$$E_{\text{pol}} = - \left[\gamma_{\text{ep}}^1 g^2 \omega_0 + \frac{\gamma_{\text{ep}}^2 t^2}{g^2 \omega_0} \right] \zeta \int_0^L dz \rho(z) [1 - a^3 \rho(z)], \quad (4)$$

where $\zeta = 6$ is the coordination number and a is the lattice constant. In arriving at the above equation we have approximated $n_{i+\delta} + n_{i-\delta} \approx 2n_i$. Furthermore, for the ground state, we expect $t_{ij} \sqrt{0.5[1 + (\mathbf{S}_i \cdot \mathbf{S}_j / S^2)]} = t_{ij}$, i.e., the minority charges will completely polarize the neighboring majority charges.

We will now minimize the total energy given below

$$E_{\text{Total}} = 2E_{\text{pol}} + 2E_{\text{coul}}, \quad (5)$$

by setting the functional derivative $\delta E_{\text{Total}} / \delta \rho(z) = 0$. This leads to the following equation

$$0 = -C_1 [1 - 2a^3 \rho(z)] + 2C_2 \int_z^L dy \left[-\tilde{E}_{\text{ext}} + \int_0^y dx \rho(x) \right], \quad (6)$$

where $C_1 \equiv \left[\gamma_{\text{ep}}^1 g^2 \omega_0 + \frac{\gamma_{\text{ep}}^2 t^2}{g^2 \omega_0} \right] \zeta$; $C_2 \equiv 2\pi e^2 / \epsilon$; and $\tilde{E}_{\text{ext}} \equiv eE_{\text{ext}} / (4\pi e)$. The above equation, upon taking double derivative with respect to z , yields

$$C_1 a^3 \frac{d^2 \rho(z)}{dz^2} - C_2 \rho(z) = 0. \quad (7)$$

The above second-order differential Eq. (7) and Eq. (6) admit the solution

$$\rho(z) = \frac{1}{2a^3} \frac{\cosh(\xi z)}{\cosh(\xi L)} + \xi \tilde{E}_{\text{ext}} \frac{\sinh[\xi(L-z)]}{\cosh(\xi L)}, \quad (8)$$

where $\xi = \sqrt{C_2 / (C_1 a^3)}$. It is important to note that, for the manganese-oxide (MO) layer at the LMO-CMO interface (i.e., at $z = L$), the density is 0.5 electrons/site and that it is independent of the applied external electric field and the system parameters. Now, since each Mn site in the interface layer belongs to a unit cell that is half LMO and half CMO, one expects the density per site to be 0.5. Additionally, as the distance from the LMO-CMO interface increases, we observe from Eq. (8) as well as from Figs. 2 and 3 that for smaller values of C_1 , the density falls more rapidly while the density change due to electric field rises faster. Furthermore, for realistic values of the parameters, the charge density rapidly changes as we move away from the oxide-oxide interface (i.e., after only a few layers from the interface) and attains values close to the bulk value [as illustrated in Figs. 2(a) and 3(a)]. Lastly, as required for zero values of the external field E_{ext} , we get $\rho(0) \rightarrow 0$ when $L \rightarrow \infty$. Thus, although we used the continuum approximation, our obtained density profile is qualitatively realistic as it has the desired values at the extremes $z = L$ and $z = 0$ with the density away from the LMO-CMO interface rapidly falling for not too large values of ϵ .

The density profiles for both LMO and CMO sides depend only on ϵ , C_1 and E_{ext} . For our calculations displayed in Fig. 2, we used the following values for the parameters: $a = 4 \text{ \AA}$; $\epsilon = 20$; $E_{\text{ext}} = 300 \text{ kV/cm}$ and 400 kV/cm ; and $C_1 = 0.24$. For Fig. 3, we employed $E_{\text{ext}} = 100 \text{ kV/cm}$ and $C_1 = 0.31$, with the values for a and ϵ being the same as in Fig. 2. The values of C_1 in Figs. 2 and 3 were chosen based on $\omega_0 = 0.07 \text{ eV}$; $g = 2$; and $t = 0.1 \text{ eV}$.

C. Magnetization distribution

We will now obtain the magnetization for a heterostructure by considering its lattice structure unlike the case for the density profile where a continuum approximation was made. Thus we can take into account the possibility of antiferromagnetic (AFM) order besides being able to consider ferromagnetic (FM) order.

First, based on Ref. 37, we note that the bulk $\text{La}_{1-x}\text{Ca}_x\text{MnO}_3$ (below the magnetic transition temperatures) is A-AFM for $0 \leq x \lesssim 0.1$ and a ferromagnet for $0.1 \lesssim x \lesssim 0.5$. Hence, we model the LMO side of the heterostructure as an A-AFM when hole concentrations are small; whereas at higher concentrations of holes which is less than 0.5, the holes dictate the magnetic order by forming magnetic polarons that polarize the A-AFM. Next, we note that for $0.5 \lesssim x \lesssim 1.0$, the $\text{La}_{1-x}\text{Ca}_x\text{MnO}_3$ bulk system is always an antiferromagnet. Thus, from a magnetism point-of-view, the magnetic moment on the CMO side of the heterostructure is expected to be zero except in the vicinity of the interface where (due to proximity effect) it will be a ferromagnet and can be modeled using a percolation picture. Given the above scenario, as can be expected, we find that the ferromagnetic region on the LMO side can be drastically enhanced (at the expense of the A-AFM region) by an electric field inducing holes on the LMO side. On the other hand, the electric field has only a small effect on the percolating ferromagnetic cluster that is adjacent to the oxide-oxide interface on the CMO side.

1. CMO side

We will first consider the CMO side and show that the magnetization decays as we move away from the LMO-CMO interface. We derive below the largest FM domain; this domain percolates from the LMO-CMO interface. On account of nearest-neighbor repulsion (as given in Eq. (1)), the interface (which is half-filled) has e_g electrons on alternate sites. In fact, to minimize the interaction energy, on the CMO side we take the e_g electrons to be in one sublattice only which will be called e_g -sublattice; the other unoccupied sublattice will be called the u -sublattice. On account of virtual hopping, an e_g electron polarizes all its neighboring sites that do not contain any e_g electrons and forms a magnetic polaron.

Thus we observe that the half-filled interface will be fully polarized and that there will be an FM cluster that begins at the interface and percolates to the layers away from the interface on the CMO side. For instance, in the layer next to the oxide-oxide interface, all the e_g electrons are in the same sublattice (the e_g -sublattice) and

are next to the empty sublattice (i.e., sublattice unoccupied by e_g electrons) of the interface and hence are ferromagnetically aligned with the interface. Similarly, again in the layer adjacent to LMO-CMO interface, all the sites in the other sublattice (i.e., the u -sublattice) are empty and have the same polarization as the sites occupied by the e_g electrons at the interface.

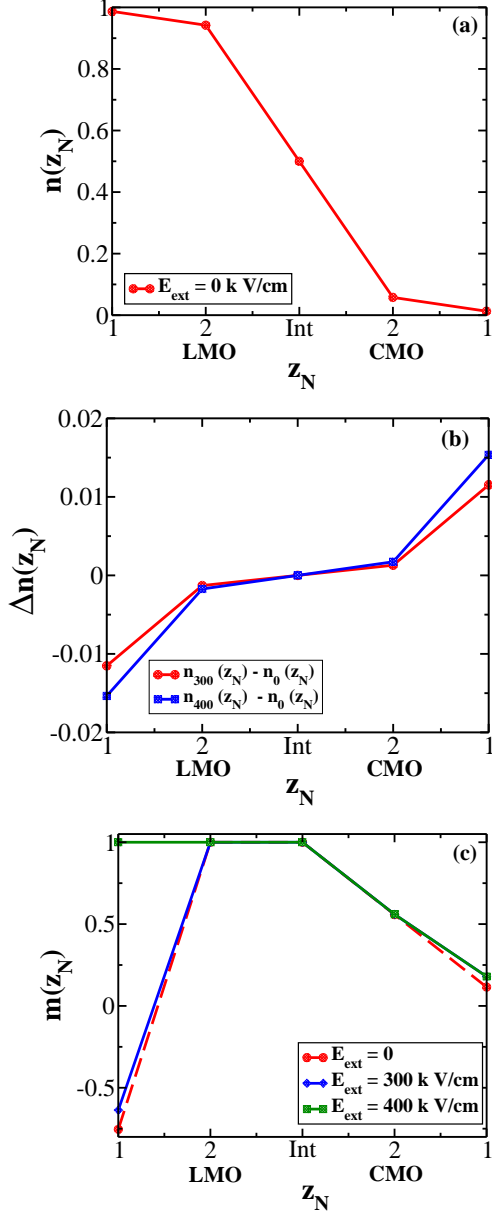


FIG. 2. (Color online) Electronic charge density $n(z_N)$ and per-site magnetization $m(z_N)$ (of t_{2g} spins normalized to unity) in various manganese-oxide layers of a (Insulator)/(LaMnO₃)₂/Interface/(CaMnO₃)₂/(Insulator) heterostructure for $a = 4$ Å, $\epsilon = 20$, and $C_1 = 0.24$. Figures are for (a) $n(E_{\text{ext}} = 0$ kV/cm); (b) $\Delta n = n(E_{\text{ext}} = 300/400$ kV/cm) $- n(E_{\text{ext}} = 0$ kV/cm); and (c) $m(z_N)$ at $E_{\text{ext}} = 0$ kV/cm, 300 kV/cm, and 400 kV/cm. MO layer 1 on the LMO side undergoes spin reversal when $E_{\text{ext}} = 400$ kV/cm is applied.

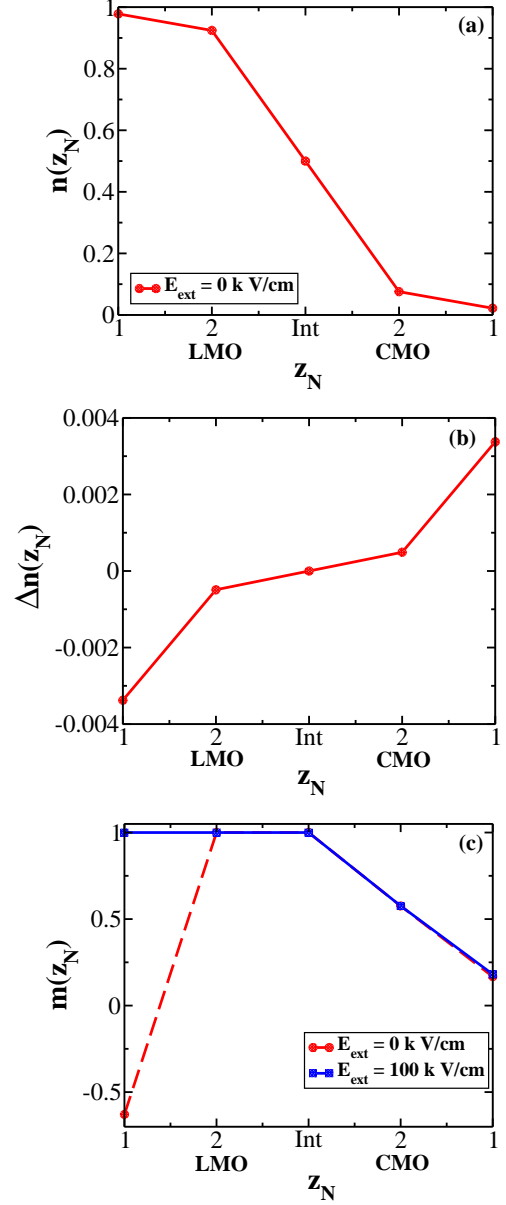


FIG. 3. (Color online) Electronic charge density $n(z_N)$ and per-site magnetization $m(z_N)$ (of normalized- t_{2g} spins) in various manganese-oxide layers of a (Insulator)/(LaMnO₃)₂/Interface/(CaMnO₃)₂/(Insulator) heterostructure for $a = 4$ Å, $\epsilon = 20$, and $C_1 = 0.31$. Plots pertain to (a) $n(E_{\text{ext}} = 0$ kV/cm); (b) $\Delta n = n(E_{\text{ext}} = 100$ kV/cm) $- n(E_{\text{ext}} = 0$ kV/cm); and (c) $m(z_N)$ at $E_{\text{ext}} = 0$ kV/cm and $E_{\text{ext}} = 100$ kV/cm. The LMO side becomes completely ferromagnetic when $E_{\text{ext}} = 100$ kV/cm is applied.

We will now identify the equations governing the ferromagnetic cluster percolating from the interface. Let z_N be the z -coordinate of the N^{th} 2D MO layer with N being the index measured from the Insulator-CMO interface (as shown in Fig. 1). Furthermore, we define $x_N^{e_g}$ (x_N^u) as the concentration of polarized sites that belong to the spanning cluster and these sites are a subset of the sites in the e_g -sublattice (u -sublattice) in the N^{th} 2D MO layer. Then, the factor $(1 - 2x_N^{e_g}) [(1 - 2x_N^u)]$ represents the probability of a site that belongs to the e_g -sublattice (u -sublattice) in layer N but is not part of the spanning polarized cluster. Now, the probability that a site, occupied (unoccupied) by an e_g electron, contributes to the FM cluster is equal to the probability of finding the site occupied (unoccupied) multiplied by $1-P$ where P is the probability that none of the adjacent sites that are in the u -sublattice (e_g -sublattice) belong to the percolating cluster. Therefore, we obtain the following set of coupled equations for the spanning cluster:

$$x_N^{e_g} = \rho(z_N)[1 - (1 - 2x_{N-1}^u)(1 - 2x_N^u)^4(1 - 2x_{N+1}^u)], \quad (9)$$

$$x_N^u = 0.5[1 - (1 - 2x_{N-1}^{e_g})(1 - 2x_N^{e_g})^4(1 - 2x_{N+1}^{e_g})]. \quad (10)$$

The boundary conditions involving layer 1 are

$$x_1^{e_g} = \rho(z_1)[1 - (1 - 2x_1^u)^4(1 - 2x_2^u)], \quad (11)$$

and

$$x_1^u = 0.5[1 - (1 - 2x_1^{e_g})^4(1 - 2x_2^{e_g})], \quad (12)$$

while those for the LMO-CMO interface are $x_{\text{Int}}^{e_g} = x_{\text{Int}}^u = 0.5$.

2. LMO side

Next, we will show that the LMO side with only a few layers, for some realistic values of parameters, can have a sizeable change in the magnetism when a large electric field is applied and thus can be exploited to obtain a giant magneto-electric effect. Similar to the bulk situation in LaMnO_3 ^{43,47}, in our heterostructure as well, we assume that two spins on any adjacent sites in each MO layer have a ferromagnetic coupling $J_{xy} = 1.39$ meV; whereas, any two neighboring spins on adjacent layers have an antiferromagnetic coupling $J_z = 1.0$ meV. On the other hand, for an electron and a hole on neighboring sites either in the same MO layer or in adjacent MO layers, (due to virtual hopping of electron between the two sites) there is a strong ferromagnetic coupling $J_{eh} = \gamma_{ep}^2 t^2 / (g^2 \omega_0) \gg J_{xy}$ ⁴². In our calculations, as long as the ratio of J_{xy}/J_z is taken as fixed and J_{eh} is the significantly dominant coupling, we get the same magnetic picture.

In a LMO side with a few MO layers, to demonstrate the possibility of large magnetization change upon the

application of a large external field, we assume that the LMO-CMO interface and all MO layers up to layer M are completely polarized. Next, we assume that MO layers M and $M-1$ have low density of holes so that there is a possibility that spins in MO layer $M-1$ are not aligned with the block of MO layers starting from the LMO-CMO interface and up to layer M . We then analyze the polarization of MO layer $M-1$ by comparing the energies for the following two cases: (i) layers $M-1$ and M are antiferromagnetically aligned with the holes in layers M and $M-1$ inducing polarization only on sites that are adjacent to the holes; and (ii) MO layer $M-1$ is completely polarized and aligned with Layer M .

In a few-layered heterostructure (Ins.)/(LaMnO_3)₂/Int./(CaMnO_3)₂/(Ins.), for $C_1 = 0.24$ eV [as shown in Fig. 2(c)] and for $C_1 = 0.31$ [as in Fig. 3(c)], we obtain a striking magneto-electric effect. For zero external field, when $M = 2$ is considered, case (i) (mentioned above) has lower energy, i.e., layer 1 is antiferromagnetically coupled to layer 2. On the other hand, when a strong electric field (~ 100 kV/cm for $C_1 = 0.24$ and ~ 400 kV/cm for $C_1 = 0.31$) is applied, MO layer 1 (due to increased density of holes) becomes completely polarized and ferromagnetically aligned with the rest of the layers (i.e., MO layer 2 and the oxide-oxide interface) on the LMO side. Thus, we get a giant magneto-electric effect! We have considered C_1 values ranging from 0.24 to 0.31 and obtained magnetoelectric effect for various threshold electric field values. Changing C_1 is physically equivalent to changing the effective nearest-neighbor electron-hole attraction. Thus a smaller C_1 value of 0.24 indicates a lower effective nearest-neighbor electron-electron repulsion which requires a larger external electric field strength of 400 kV/cm to generate enough holes on the LMO side and, consequently, flip the magnetization of layer 1. Obviously, for the larger value $C_1 = 0.31$, sufficient number of holes are already present in the LMO system and layer 1 becomes ferromagnetic when a smaller E_{ext} ($= 100$ kV/cm) is applied. At still larger values of C_1 , i.e., $C_1 \geq 0.32$, the LMO side is completely ferromagnetic even in the absence of an external field.

III. NUMERICAL APPROACH

Here, in this section, we construct a detailed 2D model Hamiltonian and study it numerically for the charge and magnetic profiles and the coupling between them. Our (Ins.)/(LaMnO_3)_n/Int./(CaMnO_3)_n/(Ins.) heterostructure depicted in Fig. 1, for the treatment in this section, involves even number of MnO_2 planes. Here we can have the following arrangement:

Ins./(LaO-MnO_2)_n/($\text{La}_{1/2}\text{Ca}_{1/2}\text{O}$)/($\text{MnO}_2\text{-CaO}$)_n/Ins. Here, the Interface is composed of $\text{La}_{1/2}\text{Ca}_{1/2}\text{O}$ (which is non-magnetic) and has 0.5 +ve charge per unit $\text{La}_{1/2}\text{Ca}_{1/2}\text{O}$. There is no polar catastrophe as any excess charge at the Ins./ LaO interface can be neutralized

by a gate potential. Each unit cell on LMO side, comprising of $[(\text{LaO})_{1/2}\text{MnO}_2(\text{LaO})_{1/2}]$, is charge neutral.

A. Model Hamiltonian

In a q2D heterostructure (involving only a few 2D layers of both manganites), as mentioned in Sec. II, we expect only a single narrow-width polaronic band to be relevant⁴². For our numerical treatment of a 2D lattice (with l_1 rows and l_2 columns), we employ the following one-band Hamiltonian:

$$H = H_{\text{KE}} + H_{\text{pol}}^{\text{mf}} + H_{\text{SE}} + H_{\text{coul}} + H_{\text{V}}. \quad (13)$$

The kinetic energy term H_{KE} is given by

$$H_{\text{KE}} = -te^{-g^2} \sum_{\langle i,j \rangle} \left[\cos\left(\frac{\theta_{ij}}{2}\right) c_i^\dagger c_j + \text{H.c.} \right], \quad (14)$$

where t is the hopping amplitude that is attenuated by the electron-phonon coupling g and c_j is the e_g electron destruction operator; furthermore, $\cos(\theta_{ij})$ is the modulation due to infinite Hund's coupling between the itinerant electrons and the localized t_{2g} spins with θ_{ij} being the angle between two localized $S = 3/2$ spins at sites i and j ^{48,49}. As mentioned in Ref. 42, in a two-band picture, for intermediate-bandwidth systems such as LCMO, the upper broad band becomes relevant in three dimensions (3D) at lower temperatures. In q2D, the upper band does not overlap with the lower polaronic band where essentially all the electrons are localized; in q2D, width of the upper band is two-thirds the width of the upper band in 3D. In narrow-band systems such as $\text{Pr}_{1-x}\text{Ca}_x\text{MnO}_3$ (PCMO), no metallic nature is observed for $x < 0.5$; we infer that the upper band in PCMO does not overlap with the lower band even at low temperatures. The width of the upper band of PCMO in 3D is about two-thirds that of LCMO in 3D. Thus, we are justified in considering a very narrow single band in our LMO-CMO heterostructure.

The second term $H_{\text{pol}}^{\text{mf}}$ in Eq. (13) is the mean-field version of H_{pol} in Eq. (1) and is expressed as

$$H_{\text{pol}}^{\text{mf}} = - \left[\gamma_{\text{ep}}^1 g^2 \omega_0 + \frac{\gamma_{\text{ep}}^2 t^2 \cos^2\left(\frac{\theta_{ij}}{2}\right)}{g^2 \omega_0} \right] \times \sum_{i,\delta} [n_i - 2n_i \langle n_{i+\delta} \rangle + \langle n_i \rangle \langle n_{i+\delta} \rangle], \quad (15)$$

where $\langle n_i \rangle \equiv \langle c_i^\dagger c_i \rangle$ refers to the mean number density at site i . A derivation of $H_{\text{KE}} + H_{\text{pol}}$ is given in Ref. 46; however, for simplicity, here we have ignored the effect of next-nearest-neighbor hopping. The next term H_{SE} in Eq. (13) pertains to the superexchange⁵⁰ term which generates A-AFM in LaMnO_3 and G-AFM in CaMnO_3 ; thus on the LaMnO_3 side, it is given by

$$H_{\text{SE}}^{\text{lmo}} = -J_{\text{xy}} \sum_{\langle i,j \rangle_{\text{xy}}} \cos(\theta_{ij}) + J_z \sum_{\langle i,j \rangle_z} \cos(\theta_{ij}), \quad (16)$$

while on the CaMnO_3 side, we express it as

$$H_{\text{SE}}^{\text{cmo}} = J_z \sum_{\langle i,j \rangle} \cos(\theta_{ij}). \quad (17)$$

In the above superexchange expressions, the magnitude of the $S = 3/2$ spins is absorbed in the superexchange coefficients J_{xy} and J_z . Our magnetic picture reproduces the bulk behavior in LMO and CMO in regions away from the holes. In bulk LCMO, at intermediate doping $0.1 < x < 0.5$, the region is ferromagnetic; this can be explained as due to an electron and a hole on adjacent sites being ferromagnetically coupled (see Ref. 42). Similar to the bulk, in our heterostructure as well, a strong ferromagnetic interaction exists between a NN electron-hole pair; this ferromagnetic interaction is much stronger than the magnetic interactions corresponding to A-AFM and G-AFM. Thus (unlike in Ref. 34, where the boundary conditions are enforced to be A-AFM on LMO side and G-AFM on CMO side), we assume A-AFM on LMO side and G-AFM on CMO side in regions that do not contain any minority carriers (i.e., holes on LMO side and electrons on CMO side).

In Eq. (13), the Coulomb interaction is accounted for through the term H_{coul} as follows:

$$H_{\text{coul}} = V_s \sum_i n_i + \alpha t \sum_{i \neq j} \left[n_i \left(\frac{\langle n_j \rangle - Z_j}{|\vec{r}_i - \vec{r}_j|} \right) - \frac{\langle n_i \rangle \langle n_j \rangle}{2|\vec{r}_i - \vec{r}_j|} \right], \quad (18)$$

where the first term on the right hand side (RHS) is actually the on-site Coulomb interaction between an electron and a positive ion that yields the bound state of an electron and is therefore applicable only to the LMO side. The remaining term on the RHS of Eq. (18), denotes long-range, mean-field Coulomb interactions between electrons as well as between electrons and positive ions. Here, Z_j represents the positive charge density operator with a value of either 1 or 0 and $|\vec{r}_i - \vec{r}_j|$ is the distance between lattice sites i and j . Furthermore, the dimensionless parameter $\alpha = \frac{e^2}{4\pi\epsilon a t}$ determines the strength of the Coulomb interaction. Lastly, in Eq. (13), the term H_{V} represents the potential felt at various sites due to an externally applied potential difference (V_{ext}) between the two insulator edges (see Fig. 1):

$$H_{\text{V}} = V_{\text{ext}} \sum_{\text{I}=1}^{l_2} \sum_{\text{K}=1}^{l_1} \left[1 - \left(\frac{\text{I} - 1}{l_2 - 1} \right) \right] n_{\text{I}+(\text{K}-1)l_2}, \quad (19)$$

where I represents the layer (or column) index with l_2 denoting the number of layers, i.e., the number of sites in the z-direction; K represents the row index with l_1 denoting the number of rows, i.e., the number of sites in a layer.

B. Calculation procedure

We consider a 2D lattice involving a few layers (columns) of LMO and CMO and study magnetoelec-

tric effect. The lattice does not have periodicity in the direction normal to the interface of the heterostructure (i.e., the z -direction). On the other hand, to mimic infinite extent in the direction parallel to the interface of the heterostructure, we assume periodic boundary condition in that direction. We employ classical Monte Carlo with Metropolis update algorithm to obtain the charge and magnetic profiles for our 2D lattice. To tackle the difficult problem of several local minima that are close in energy, we take recourse to the simulated annealing technique. To arrive at a reasonable charge profile at energy scales much larger than the superexchange energy scale, we treat the problem classically (i.e., fully electrostatically) by considering only the Coulomb term (H_{coul}), the external-potential term (H_V), and the electron-phonon-interaction term [$H_{\text{pol}}^{\text{mf}}(\theta_{ij} = 0)$] as these are the dominant energy terms in the Hamiltonian. The Coulomb term is subjected to mean-field analysis (as mentioned before) and the system generated potential $\alpha t \sum_{i \neq j} \left\{ \frac{\langle n_j \rangle - Z_j}{|\vec{r}_i - \vec{r}_j|} \right\}^{51}$ in Eq. (18) is solved self-consistently. This is equivalent to solving the Poisson equation⁵².

Next, to arrive at the final charge and magnetic configurations, we treat the system quantum mechanically by starting with an initial configuration comprising of the charge configuration generated classically (by the above procedure) and an initial random spin configuration. We now consider the full Hamiltonian, where hopping term (H_{KE}) and spin interaction energy act as perturbation to the classical dominant energy terms [H_{coul} , H_V , and $H_{\text{pol}}^{\text{mf}}(\theta_{ij} = 0)$], thereby allowing for a small change in the number density profile and determine the concomitant magnetic profile. For the classical t_{2g} spins $\vec{S}_i = (\sin \theta_i \cos \phi_i, \sin \theta_i \sin \phi_i, \cos \theta_i)$ that are normalized to unity, the $\cos(\theta)$ and ϕ values are binned in the intervals $(-1, 1)$ and $(0, 2\pi)$ respectively with equally spaced 40 values of $\cos(\theta)$ and 80 values of ϕ , hence yielding a total of 3200 different possibilities.

In our calculations, we employ the parameter values $t = 0.1$ eV, $g = 2$ & 2.2 , and $\omega_0 = 0.07$ leading to a small parameter value $\frac{t}{\sqrt{2}g\omega_0} < 1$. For our manganite heterostructure, lattice constant $a = 4$ Å, dielectric constant $\epsilon = 20$, magnetic couplings $J_z = 1.00$ meV and $J_{xy}/J_z = 1.39$; we take the pre-factors [in Eq. (15)] $\gamma_{ep}^1 = 0.3$ and $\gamma_{ep}^2 = 0.25$. The coefficient in Eq. (18) is taken to be $V_s = -3\alpha$ for $\epsilon = 20$; hence the confining radius for the e_g electron is 1.33 Å which is less than half the lattice constant^{53,54}. It is important to point out that, since the work function (WF) of CaMnO_3 is larger than the WF of LaMnO_3 (by about 1 eV as given in Table IV of Ref. 57), we get electrons flowing from LaMnO_3 to CaMnO_3 ⁵⁸. We approximate $\text{WF}_{\text{CMO}} - \text{WF}_{\text{LMO}}$ to be given by the sum of the nearest-neighbor repulsions due to electron-phonon coupling [which is order of polaron-energy \times coordination-number] and the on-site Coulomb energy V_s . External potential differences V_{ext} , corresponding to external electric fields $E_{\text{ext}} =$

300 kV/cm and $E_{\text{ext}} = 400$ kV/cm (which are less than the breakdown field in LCMO ⁵⁹), are applied to study changes in the magnetization profiles.

The simulation (involving the charge and spin degrees of freedom) is carried out using exact diagonalization of the total Hamiltonian in Eq. (13). The spins are annealed over 61 values of the dimensionless temperature [$k_B T / (te^{-g^2})$], in steps of 0.05, starting from 3 and ending at 0.05 with 15000 system sweeps carried out at each temperature. Since hopping energy $te^{-g^2} > J_{xy}$, the inclusion of the spin degrees of freedom certainly commences at temperatures $k_B T > J_{xy}$. Furthermore, the endpoint $k_B T = 0.05te^{-g^2}$ is sufficiently small to correspond to the ground state of the system. Each sweep requires visiting all the lattice sites sequentially and updating the spin configuration at each lattice site by the standard Metropolis Monte Carlo algorithm. We are also allowing the charge degrees of freedom to relax by treating the problem self-consistently. So, at the beginning of each sweep, the Poisson equation is solved additionally to make sure that the number densities have converged and this is achieved with an accuracy of 0.001. Finally, averages of the various measurables in the system are taken over the last 5000 sweeps in the system.

C. Results and discussion

For numerical simulation, we consider two lattice sizes, namely, 12×6 and 12×8 with number of rows $l_1 = 12$ and number of layers (columns) $l_2 = 6$ or 8 . Here, all the Mn sites in each layer belong solely to either LMO or CMO. This is in contrast to the continuum approximation employed in Sec. II B to obtain the charge profile analytically. In Sec. II B, by exploiting the symmetry of the interactions of the minority carriers on both sides of the LMO-CMO interface, we derived the charge profile with charge density always $\langle n \rangle = 0.5$ at the interface; this corresponds to a system comprising of odd number of MnO_2 layers with the interface MnO_2 layer being shared equally by the LMO and CMO sides.

We consider various situations in our lattices. First, we analyze the case of excluding electron-phonon interaction; consequently, the Hamiltonian of interest is that given by Eq. (13), but without the $H_{\text{pol}}^{\text{mf}}$ term. Next, we study the charge and magnetic profiles predicted by the total Hamiltonian of Eq. (13) for the symmetric situation (of equal number of LMO and CMO layers) and for different sizeable values of the electron-phonon coupling, i.e., for $g = 2$ & 2.2 . Lastly, we examine the impact on the magnetoelectric effect due to the asymmetry in number of LMO and CMO layers.

1. No electron-phonon interaction and $E_{\text{ext}} = 400$ kV/cm

Here, without the electron-phonon interaction, the hopping amplitude t is not attenuated by the factor e^{-g^2} and the ground state is a superposition of various states in the occupation number representation. The electrons are not localized and we do not need to employ simulated annealing; the calculations were performed at a single temperature $k_B T = 0.001t$ on a symmetric heterostructure defined on a lattice with equal number of layers on the LMO side and the CMO side. Furthermore, the charge density profile is essentially dictated by the Coulombic term in Eq. (13); the kinetic term and the superexchange term have a negligible effect. Thus, we have density close to 1 on the LMO side and an almost zero density on the CMO side. Now, when a large electric field (400 kV/cm) is applied, a small amount of charge gets pushed across the interface. Then, since the kinetic term is much larger than the superexchange term, double exchange tries to ferromagnetically align the spins and, as shown in Fig. 4, we get a large change in the total magnetization of t_{2g} spins of the system, i.e., 0.91/site for the 12×8 lattice when t_{2g} spins are normalized to unity.

Keeping the temperature fixed at $0.001t$, if we now double the value of J_z to $0.02t$ while retaining the magnetic-coupling ratio $J_{xy}/J_z = 1.39$, it is found that that the magnetoelectric effect disappears completely. Owing to the larger superexchange interaction, there is only a small change in the density on the LMO and CMO sides. Consequently, superexchange dominates over double exchange, thereby making the system totally antiferromagnetic (i.e., similar to the bulk, the LMO side is A-AFM and the CMO side is G-AFM). Furthermore, even after the application of a large external electric field (i.e., $E_{\text{ext}} = 400$ kV/cm), there is practically no change in the magnetization as demonstrated in Fig. 5.

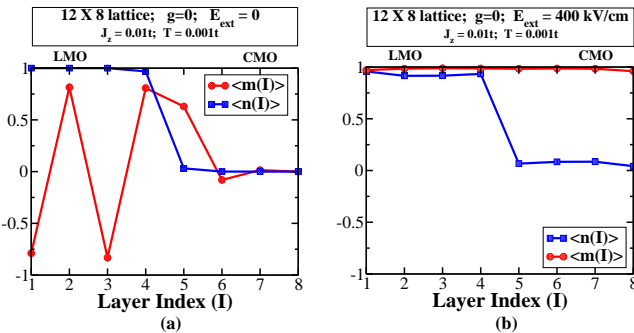


FIG. 4. (Color online) Layer-averaged charge density $\langle n(I) \rangle$ and layer-averaged per-site magnetization $\langle m(I) \rangle$ (of t_{2g} spins normalized to unity) for a symmetric 12×8 LMO-CMO lattice when electron-phonon interaction is zero; $J_z = 0.01t$ and $J_{xy}/J_z = 1.39$; $T = 0.001t$; and when (a) external electric field $E_{\text{ext}} = 0$ and (b) $E_{\text{ext}} = 400$ kV/cm.

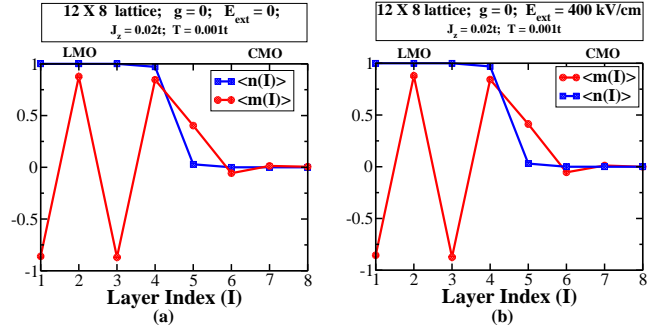


FIG. 5. (Color online) Layer-averaged charge density $\langle n(I) \rangle$ and layer-averaged per-site magnetization $\langle m(I) \rangle$ (of t_{2g} spins normalized to unity) for a symmetric 12×8 LMO-CMO lattice when electron-phonon interaction $g = 0$; superexchange $J_z = 0.02t$ and coupling ratio $J_{xy}/J_z = 1.39$; $T = 0.001t$; and when (a) $E_{\text{ext}} = 0$ and (b) $E_{\text{ext}} = 400$ kV/cm.

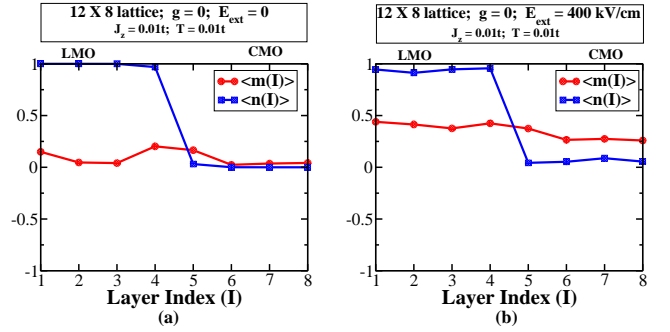


FIG. 6. (Color online) Layer-averaged charge density $\langle n(I) \rangle$ and layer-averaged per-site magnetization $\langle m(I) \rangle$ (of normalized-to-unity t_{2g} spins) for a symmetric 12×8 LMO-CMO lattice when $g = 0$; $J_z = 0.01t$ and $J_{xy}/J_z = 1.39$; enhanced temperature $T = 0.01t$; and when (a) $E_{\text{ext}} = 0$ and (b) $E_{\text{ext}} = 400$ kV/cm.

Next, on retaining the superexchange interaction values of $J_z = 0.01t$ and $J_{xy}/J_z = 1.39$, when the temperature is increased from $0.001t$ to $0.01t$, the disordering effect of the temperature dominates over superexchange making the magnetic profile lose its oscillatory nature on the LMO side [as can be seen by comparing Fig. 6(a) with Fig. 4(a)]. On the application of a sizeable external electric field (i.e., $E_{\text{ext}} = 400$ kV/cm), minority carrier density increases on both LMO and CMO sides. However, the disordering effect of the enhanced temperature diminishes the double exchange effect, thereby producing only a modest increase in the magnetization on both the LMO and CMO sides [see Fig. 6(b) and Fig. 4(b)].

In manganites the electron-phonon interaction is quite strong and leads to sizeable cooperative oxygen octahedra distortions. Hence, to get a more realistic picture, we switch on this interaction and study its effect on the system. Then, the hopping amplitude t is attenuated by the factor e^{-g^2} and the electrons are essentially localized. Consequently, the states are more or less classical

in nature with number density at each site close to 1 (i.e., > 0.99 from our calculations) or close to 0 (i.e., < 0.01 from our numerics); the state of the system can be represented by a single state in the occupation number representation. As discussed in Sec. III B, we employ simulated annealing; we arrive at the charge and magnetic profiles reported in the subsequent Secs. III C 2–III C 6.

2. Symmetric 12×8 lattice with $g = 2.0$ and $E_{\text{ext}} = 300 \text{ kV/cm}$

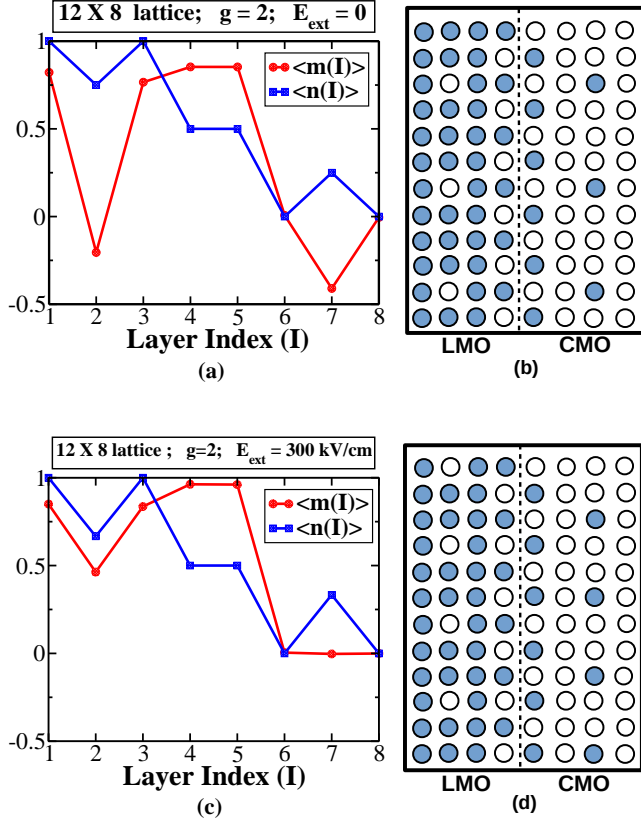


FIG. 7. (Color online) In a 12×8 symmetric lattice, when electron-phonon interaction strength $g = 2.0$, (a) when external electric field $E_{\text{ext}} = 0$, layer-averaged profiles of charge density $\langle n(I) \rangle$ and magnetization $\langle m(I) \rangle$ (of the t_{2g} spins normalized to unity); (b) when external electric field $E_{\text{ext}} = 0$, schematic occupation-number representation of ground state charge configuration in the lattice; (c) when a large external electric field $E_{\text{ext}} = 300 \text{ kV/cm}$ is applied, modified layer-averaged charge density $\langle n(I) \rangle$ and layer-averaged magnetization $\langle m(I) \rangle$ (of the t_{2g} spins normalized to unity) for various layers in the lattice; and (d) when $E_{\text{ext}} = 300 \text{ kV/cm}$, reorganized ground state charge configuration.

We now consider a symmetric 12×8 lattice with 4 layers of LMO and another 4 layers of CMO as shown in Fig. 7. We find charge modulation in the z -direction on both the sides, with neutral layers (free of minority carriers) sandwiched between charged layers (with minority

carriers). The layers at the interface have the largest number of minority carriers with electrons and holes on alternate sites since contributions from both H_{pol} and H_{coul} [given by Eqs. (1) and (18)] are minimized for this arrangement. Layers 1 and 8, being the farthest from the LMO-CMO interface, are devoid of any minority carriers and retain the expected bulk charge distribution of LMO and CMO. We will now explain the charge modulation

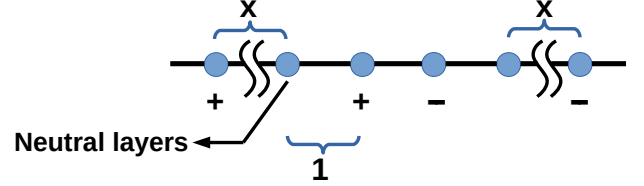


FIG. 8. (Color online) Charge modulation due to Coulomb interaction H_{coul} in a one-dimensional symmetric LMO-CMO lattice. The number of neutral layers/sites is x .

as follows. We compute the energy E_{coul} electrostatically for the one-dimensional chain in Fig. 8 using H_{coul} in Eq.(18), with lattice constant taken as unity and the number of the neutral layers/sites as x . Then

$$E_{\text{coul}} = \frac{1}{x+1} - \frac{1}{x+2} - \frac{1}{2x+3} - 1 - \frac{1}{x+2} + \frac{1}{x+1} \\ = \frac{2}{x+1} - \frac{2}{x+2} - \frac{1}{2x+3} - 1. \quad (20)$$

If we plot E_{coul} as a function of x , we find that it drops rapidly till $x = 1$ and attains its minimum value gradually somewhere between $x = 6$ and $x = 7$. Similarly, we expect neutral layers to be present in 2D also and conclude that the charge ordering sets in due to electrostatic Coulomb energy minimization.

In Fig. 7, the interface is fairly polarized since the arrangement of electrons and holes on alternate sites produces a strong ferromagnetic coupling between the spins on these sites as $J_{\text{eh}} \gg J_{\text{xy}} > J_z$. Furthermore, again due to ferromagnetic couplings J_{eh} and J_{xy} on the LMO side, the interfacial MnO_2 layer polarizes the neutral layer 3 adjacent to it. Layer 1 is polarized in the direction of layer 3 due to antiferromagnetic coupling J_z . On the CMO side, layer 6 is antiferromagnetic based on the charge configuration; layer 8, as expected, is also fully antiferromagnetic. As regards the case of zero electric field shown in Figs. 7(a) and 7(b), since layer 3 is antiferromagnetically connected to layer 2, layer 2 shows a small negative magnetization with the magnitude diminished due to the presence of a few (i.e., 3) holes in this layer. On the application of a large electric field $E_{\text{ext}} = 300 \text{ kV/cm}$, as displayed in Figs. 7(c) and 7(d), number of minority carriers increases in both layer 2 and layer 7. Consequently, the magnetization increases in these layers. On the application of the external electric field, there is an overall increase in the magnetization (of normalized-to-unity t_{2g} spins) by $0.17/\text{site}$ leading to a giant magnetoelectric effect (as can be seen in Fig. 9)

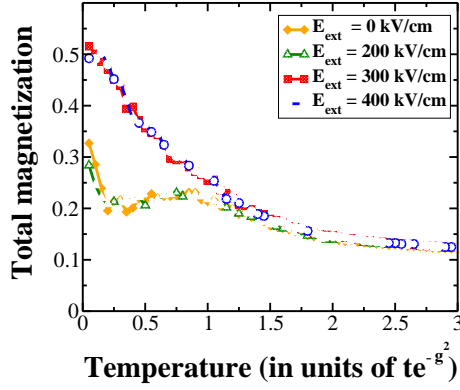


FIG. 9. (Color online) Total magnetization as a function of temperature for various E_{ext} in a 12×8 lattice when electron-phonon coupling $g = 2.0$. Figure shows that an enhancement in magnetization occurs for electric fields $E_{\text{ext}} \gtrsim 300$ kV/cm; whereas below this threshold value, total magnetization does not change from its value at $E_{\text{ext}} = 0$ kV/cm. The magnetoelectric effect is reasonably large at temperatures below $0.5te^{-g^2}$ (~ 10 K).

A study of the total magnetization with temperature for various external electric fields (i.e., E_{ext} increased in steps of 100 kV/cm from 0), as depicted in Fig. 9, reveals that we need a threshold field $\simeq 300$ kV/cm to get a fairly large increase in the total magnetization. Only above the threshold value, the density of minority charges increases and the resulting charge configuration is modified; correspondingly, the spin configuration gets altered too. Above 300 kV/cm, the charge configuration gets frozen for consecutive higher electric fields up to 600 kV/cm and no change in the magnetic profile can be expected. Although it may seem that much higher electric fields will further change the magnetization, they will actually produce a breakdown.

3. Symmetric 12×8 lattice with $g = 2.2$ and $E_{\text{ext}} = 0$

Here we would like to point out that charge and magnetic profiles, when electron-phonon coupling g is strong and external electric field is zero, are similar to the profiles when coupling g is weak and external electric field is strong. In fact, as can be seen from Fig. 10 and Figs. 7(c) and 7(d), for $g = 2.2$ and $E_{\text{ext}} = 0$ we get the same charge profile as when $g = 2.0$ and $E_{\text{ext}} = 300$ kV/cm; the corresponding magnetic profiles in the two cases differ slightly because the ferromagnetic coupling values $J_{\text{eh}} = \gamma_{\text{ep}}^2 t^2 / (g^2 \omega_0)$ are slightly different.

4. Symmetric 12×6 lattice with $g = 2.2$ and $E_{\text{ext}} = 400$ kV/cm

Since the electron-phonon interaction is stronger here (i.e., $g = 2.2$) compared to the situation in Sec. III C 2,

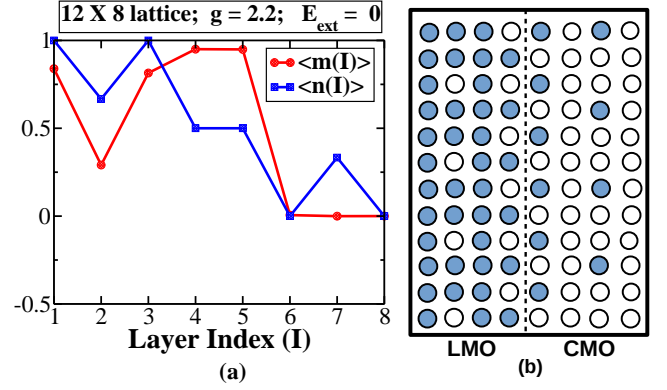


FIG. 10. (Color online) Result of enhanced electron-phonon coupling $g = 2.2$ and zero electric field, in a symmetric 12×8 lattice, on (a) layer-averaged charge density $\langle n(I) \rangle$ and layer-averaged magnetization $\langle m(I) \rangle$ (of the t_{2g} spins normalized to unity); and (b) ground state charge configuration.

even without the application of an external electric field, the concentration of minority carriers is higher (on both LMO side and CMO side) as can be seen from Figs. 11 and 7. Again, as depicted in Figs. 11(a) and 11(b), the interfacial MnO_2 layers (i.e., layers 3 and 4) have electrons and holes on alternate sites resulting in full ferromagnetism. Here, we have fewer layers compared to the case in Sec. III C 2; there is no charge modulation in the z -direction because shifting the holes from layer 2 to layer 1 increases the number of nearest-neighbor repulsions due to electron-phonon interactions. Layers 2 and 5 also have a sizeable density of minority carriers (i.e., $1/3$). Consequently, layer 2 is polarized due to its proximity to layer 3 and the ferromagnetic couplings J_{eh} and J_{xy} ; contrastingly, the combination of J_{eh} and the antiferromagnetic coupling J_z lead to a smaller polarization in layer 5. Layer 1, due to its proximity to layer 2 (with sizeable concentration of holes) is also partially polarized. On the application of a large electric field ($E_{\text{ext}} = 400$ kV/cm), as portrayed in Figs. 11(c) and 11(d), the concentration of holes further increases in layers 2 and 5 leading to fully ferromagnetically aligning these layers with layers 3 and 4. Furthermore, layer 1 also gets more polarized. On the whole, total magnetization (of normalized-to-unity t_{2g} spins) increases by $\sim 0.17/\text{site}$ thus producing a giant magnetoelectric effect.

We will now make an important observation pertaining to the positive charge (Z_j) configuration near the interface. As mentioned before for the heterostructure, we considered the following arrangement with an even number of MnO_2 planes:

Ins./ $(\text{LaO-MnO}_2)_n/(\text{La}_{1/2}\text{Ca}_{1/2}\text{O})/(\text{MnO}_2\text{-CaO})_n/\text{Ins.}$
Here, the Interface is composed of $\text{La}_{1/2}\text{Ca}_{1/2}\text{O}$ and has 0.5 +ve charge per unit $\text{La}_{1/2}\text{Ca}_{1/2}\text{O}$. In all our calculations we have used $Z_j = 1$ on the LMO side and $Z_j = 0$ on the CMO side. Now, the values of Z_j used are exact for unit cells that are not adjacent to the interface. However, for the unit cell adjacent to the in-

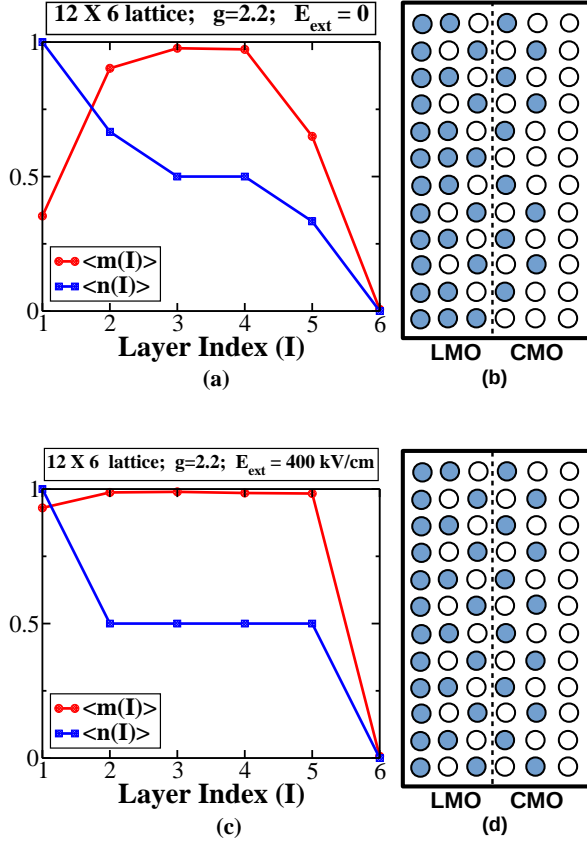


FIG. 11. (Color online) In a symmetric 12×6 lattice, for enhanced coupling $g = 2.2$, (a) at zero electric field, layer-averaged charge density $\langle n(I) \rangle$ and layer-averaged magnetization $\langle m(I) \rangle$ of t_{2g} spins normalized to unity; (b) at $E_{\text{ext}} = 0$, ground state configuration; (c) at strong external electric field $E_{\text{ext}} = 400$ kV/cm, layer-averaged charge density $\langle n(I) \rangle$ and layer-averaged magnetization $\langle m(I) \rangle$ of t_{2g} spins normalized to unity; and (d) at $E_{\text{ext}} = 400$ kV/cm, charge configuration in the ground state.

interface on the LMO (CMO) side $Z_j = 1$ ($Z_j = 0$) is an approximation and strictly speaking it should be $Z_j = 0.75$ ($Z_j = 0.25$) as will be explained below. Each unit cell on the LMO side, excluding the unit cell at the interface, comprises of $[(\text{LaO})_{1/2}\text{MnO}_2(\text{LaO})_{1/2}]$ and has 1 +ve charge, i.e., $Z_j = 1$; on the other hand, $[(\text{LaO})_{1/2}\text{MnO}_2(\text{La}_{1/2}\text{Ca}_{1/2}\text{O})_{1/2}]$ is the unit cell at the interface on the LMO side and has 0.75 +ve charge, i.e., $Z_j = 0.75$. Next, on the CMO side, excluding the unit cell at the interface, each unit cell comprises of $[(\text{CaO})_{1/2}\text{MnO}_2(\text{CaO})_{1/2}]$ and has 0 +ve charge, i.e., $Z_j = 0$; contrastingly, $[(\text{La}_{1/2}\text{Ca}_{1/2}\text{O})_{1/2}\text{MnO}_2(\text{CaO})_{1/2}]$ is the unit cell at the interface on the CMO side and has 0.25 +ve charge, i.e., $Z_j = 0.25$. Thus, at the interface we have the situation $Z_j = 0.75|Z_j = 0.25$ instead of $Z_j = 1|Z_j = 0$ as previously assumed⁶⁰.

We will now demonstrate that, even if intermixing of La and Ca ions is allowed to obtain $Z_j = 0.75|Z_j = 0.25$ at the interface, ground state charge configuration iden-

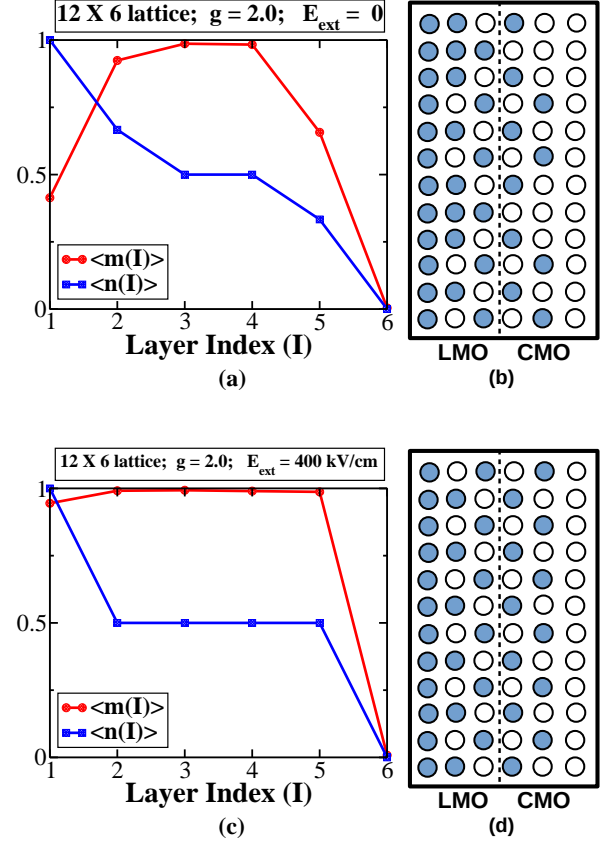


FIG. 12. In a symmetric 12×6 lattice, for reduced coupling $g = 2.0$ and for the heterostructure $\text{Ins.}/(\text{LaO-MnO}_2)_n/(\text{La}_{1/2}\text{Ca}_{1/2}\text{O})/(\text{MnO}_2\text{-CaO})_n/\text{Ins.}$ with $Z_j = 0.75$ ($Z_j = 0.25$) for the layer adjacent to interface on the LMO (CMO) side, (a) at zero electric field, layer-averaged charge density $\langle n(I) \rangle$ and layer-averaged magnetization $\langle m(I) \rangle$ of t_{2g} spins normalized to unity; (b) at $E_{\text{ext}} = 0$, ground state configuration; (c) at strong external electric field $E_{\text{ext}} = 400$ kV/cm, layer-averaged charge density $\langle n(I) \rangle$ and layer-averaged magnetization $\langle m(I) \rangle$ of t_{2g} spins normalized to unity; and (d) at $E_{\text{ext}} = 400$ kV/cm, charge configuration in the ground state.

tical to that of the $Z_j = 1|Z_j = 0$ case can be obtained for a slightly lower strength of electron-phonon interaction (i.e., lower nearest-neighbor repulsion) when the same external electric field is employed; this is because the electrons are less confined to the LMO side in the $Z_j = 0.75|Z_j = 0.25$ case. Consequently, as shown in Fig. 12, a slightly smaller magnetoelectric effect is observed. We note that V_s is scaled proportional to the values of Z_j in the two lattice layers at the interface. For the $Z_j = 0.75|Z_j = 0.25$ case, we find that there is an overall increase in the magnetization (of normalized-to-unity t_{2g} spins) by 0.16/site (implying a giant magnetoelectric effect) which is only slightly smaller than the previous result of 0.17/site for the $Z_j = 1|Z_j = 0$ case. To get the same ground state charge configuration ob-

tained when $g = 2.2$ for the $Z_j = 1|Z_j = 0$ case, a lower electron-phonon strength of $g = 2$ suffices for the $Z_j = 0.75|Z_j = 0.25$ case.

From the magnetization profile in Fig. 12, for the situations when an external electric field is not applied as well as when it is applied, one can clearly see that there is in general a slight increase in the magnetization for all the layers in the $Z_j = 0.75|Z_j = 0.25$ case as compared to the $Z_j = 1|Z_j = 0$ case (see Fig. 11). This is because with the lowering of the coupling g for the $Z_j = 0.75|Z_j = 0.25$ case, the strength of the polarizing part of $H_{\text{pol}}^{\text{mf}}$ (i.e., $\frac{\gamma_{\text{ep}}^2 t^2 \cos^2(\frac{\theta_{ij}}{2})}{g^2 \omega_0}$) increases; hence, the magnetizing effect of the electron-phonon interaction also gets enhanced.

Lastly, it should be noted that (as expected) the magnetic profiles obtained here in Figs. 11 and 12 are quite similar to those in Figs. 2 and 3; on the other hand, the agreement between the charge profiles is not as good. On comparing the analytic treatment with the numerical approach, we note that the former makes a continuum approximation to obtain the charge profile. If the number of layers is large compared to the lattice constant, the continuum approximation is valid and the prediction of the analytic approach will agree with the more accurate numerical one. On the other hand, for a small system such as a 12×8 system, charge modulation is generated in the numerical approach unlike the analytic case.

5. Asymmetric 12×8 system of 2 LMO layers and 6 CMO layers with $g = 2.0$ and $E_{\text{ext}} = 300$ kV/cm

We have an asymmetry here regarding the number of layers; the LMO side has two layers whereas the CMO side has six layers. For zero external electric field, as shown in Figs. 13(a) and 13(b), the two interfacial MnO_2 layers 2 and 3 contain perfectly alternate arrangement of electrons and holes; hence, the layers are fully polarized. Layer 1 is also ferromagnetically aligned with layer 2 because of their proximity. Beyond layer 3, similar to the G-AFM order in bulk CMO, the CMO side is antiferromagnetic, resulting in zero magnetization. Turning on the sizeable electric field $E_{\text{ext}} = 300$ kV/cm, as depicted in Figs. 13(c) and 13(d), leads to a few electrons from layer 1 ending up in a farther layer 7; resultantly, the magnetic polarons in layer 7 partially polarize it. It is interesting to note that, here too charge modulation occurs due to the Coulomb term H_{coul} as demonstrated through Eq. (20). There is an overall increase in the magnetization (of normalized-to-unity t_{2g} spins) by 0.04/site; thus, the magnetoelectric effect is not huge.

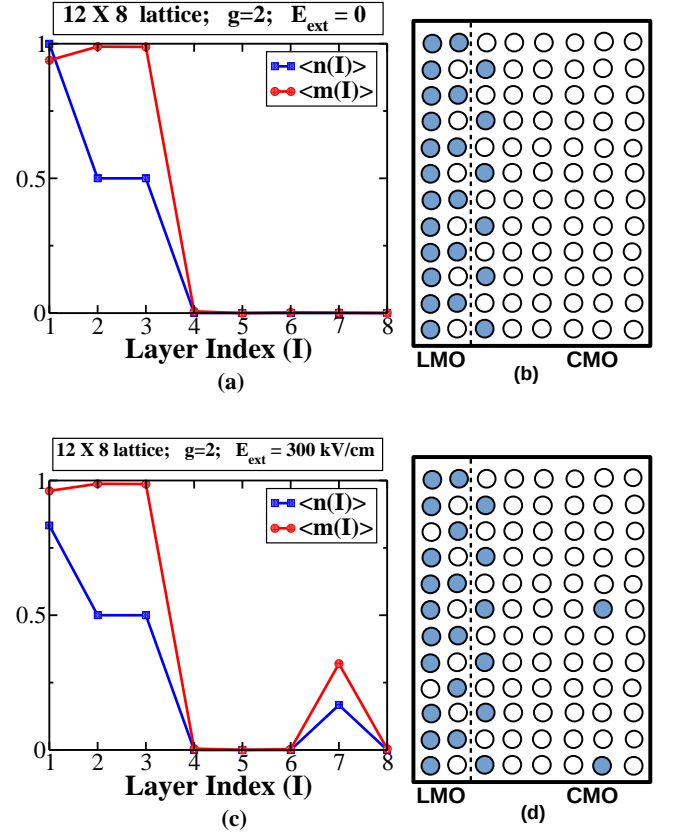


FIG. 13. (Color online) In asymmetric heterostructure defined on a 12×8 lattice with 2 layers of LMO and 6 layers of CMO, when coupling $g = 2.0$, (a) at $E_{\text{ext}} = 0$, layer-averaged charge density $\langle n(I) \rangle$ and layer-averaged magnetization $\langle m(I) \rangle$ of normalized-to-unity t_{2g} spins; (b) at $E_{\text{ext}} = 0$, ground state configuration; (c) at $E_{\text{ext}} = 300$ kV/cm, layer-averaged charge profile $\langle n(I) \rangle$ and layer-averaged magnetization profile $\langle m(I) \rangle$ of normalized-to-unity t_{2g} spins; and (d) at $E_{\text{ext}} = 300$ kV/cm, ground state configuration.

6. Asymmetric 12×8 system of 6 LMO layers and 2 CMO layers with $g = 2.0$ and $E_{\text{ext}} = 300$ kV/cm

Here, compared to the previous structure in Fig. 13, we have the opposite asymmetric structure of 6 LMO layers and 2 CMO layers (see Fig. 14). Due to the asymmetry connection between these two structures, we obtain a mirror image of the previous charge configuration for both with and without the external electric field. The interfacial MnO_2 layers 6 and 7, as expected, are totally ferromagnetic. Furthermore, layer 5 is also ferromagnetically aligned with layers 6 and 7 due to the ferromagnetic couplings J_{eh} and J_{xy} . At zero external field [as shown in Figs. 14(a) and 14(b)], similar to the bulk situation, we have A-AFM on the LMO side up to layer 5; layer 8, similar to the bulk CMO, is also antiferromagnetic. The minority carriers, generated due to the external electric field $E_{\text{ext}} = 300$ kV/cm [as shown in Figs. 14(c) and 14(d)], produce magnetic polarons which

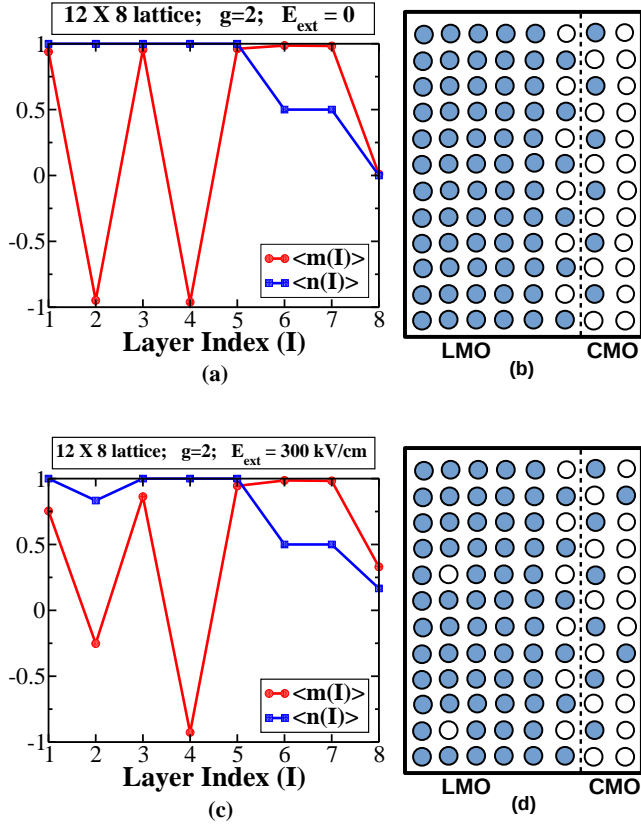


FIG. 14. (Color online) In asymmetric 12×8 lattice with 6 layers of LMO and 2 layers of CMO, when electron-phonon interaction $g = 2.0$, (a) at external electric field $E_{\text{ext}} = 0$, layer-averaged electron density $\langle n(I) \rangle$ and layer-averaged magnetization $\langle m(I) \rangle$ of t_{2g} spins normalized to unity; (b) at $E_{\text{ext}} = 0$, ground state electronic configuration; (c) at $E_{\text{ext}} = 300$ kV/cm, layer-averaged electron density $\langle n(I) \rangle$ and layer-averaged magnetization $\langle m(I) \rangle$ of t_{2g} spins normalized to unity; and (d) at $E_{\text{ext}} = 300$ kV/cm, ground state.

increase the polarization. There is an overall increase in the magnetization (of normalized-to-unity t_{2g} spins) by about 0.1/site implying a large magnetoelectric effect.

From the various symmetric and asymmetric LMO-CMO configurations considered, we conclude that the symmetric arrangement yields the largest magnetoelectric effect.

Lastly, for both symmetric and asymmetric heterostructures, the dominant charge interactions (i.e., Coulombic interaction and CEPI) lead to checkerboard order (i.e., alternating electrons and holes) for the two layers at the interface. At the interface, it is important to note that an electron in one layer is next to a hole in the next layer. This scenario is not true in the bulk $\text{La}_{1/2}\text{Ca}_{1/2}\text{MnO}_3$. In bulk $\text{La}_{1/2}\text{Ca}_{1/2}\text{MnO}_3$, in the z -direction (i.e., direction perpendicular to the planes with zigzag ferromagnetic chains that are coupled antiferromagnetically) an electron in one orbital is above another electron in the same orbital; this can support the experimentally observed CE-AFM ordering. However, for the charge or-

dering that results at the interface where an electron in one plane is next to a hole in the next plane, CE-type spin order is not possible (because ferromagnetic zigzag chains in one plane cannot lie exactly over ferromagnetic zigzag chains in the next plane). On taking the dominant charge interactions and the dominant magnetic interactions (i.e., electron and hole on adjacent sites being ferromagnetically coupled), we get ferromagnetic layers at the interface.

In Ref. 34, since they ignore CEPI (which produces large nearest-neighbor repulsion), they do not get a charge ordering where an electron in one plane at the interface is next to a hole in the next plane at the interface. Additionally, it should also be noted that, a hole (in the plane at the interface on the LMO side) prefers to be next to an electron (in the plane at the interface on the CMO side) due to attractive Coulombic interaction.

IV. CONCLUSIONS

We used the heuristic notion that, when the two Mott insulators LMO and CMO are brought together to form a heterostructure, one may realize the entire phase diagram of $\text{La}_{1-x}\text{Ca}_x\text{MnO}_3$ across the heterostructure with the $x = 0$ phase occurring at the LMO surface at one end and evolving to the $x = 0.5$ state at the oxide-oxide interface and finally to the $x = 1$ phase at the other end of CMO. However, owing to the reduced dimensions (namely, quasi two-dimensions), we expect only A-AFM and FMI phases on the LMO side. On enhancing the minority carrier density (on both sides of the interface) by using a sizeable external electric field, we showed that the FMI region can be further expanded at the expense of the A-type AFM region on the LMO side and the G-AFM domain on the CMO side, thereby producing a giant magnetoelectric effect. It is important to note that the system behaves like an anisotropic solid: for a given average density in a layer, the minority charges by and large order periodically and as far apart as possible; the Coulombic interaction and the CEPI dictate how the charge arrangement of one layer adjusts itself with respect to the configuration in another layer. Furthermore, the two layers at the interface are ferromagnetically ordered as they are at half-filling. When electric fields are introduced in the system, the minority charge density away from the interface gets enhanced leading to charge reordering; consequently, the magnetization away from the interface changes layer by layer resulting in an increase in the total ferromagnetic moment. This scenario is key to the understanding of the magnetoelectric effect.

We would like to point out that the model in Sec. III is not applicable in three dimensions because upper wide band becomes relevant (see Ref. 42); consequently, states such as the ferromagnetic metal in LCMO cannot be realized using this model. Furthermore, long-range Coulomb interactions are not very important to explain the gross features of the phase diagram in the three-dimensional

bulk system.

As a guide to designing magnetoelectric devices, we find that symmetric heterostructures with equal number of LMO and CMO layers yield larger magnetoelectric effect compared to asymmetric heterostructures with unequal number of LMO and CMO layers. It should also be noted that this heterostructure/device can be used near helium liquefaction temperatures; on the other hand, the magnetoelectric function disappears before nitrogen liquefaction temperature is attained.

We also would like to mention that if a superlattice were formed from the heterostructure $(\text{Ins.})/(\text{LaMnO}_3)_n/\text{Int.}/(\text{CaMnO}_3)_m/(\text{Ins.})$, then the dipoles from each repeating heterostructure unit will add up to produce a giant electric dipole moment; furthermore, this superlattice will also realize a giant magnetoelectric effect. On the other hand, if the insulator layers were not present, the superlattice formed from the repeating unit $(\text{LaMnO}_3)_n/(\text{CaMnO}_3)_m$ would not produce a large electric dipole as the charge from LMO can leak to CMO on both sides leading to a small net dipole moment. More importantly, the $(\text{LaMnO}_3)_n/(\text{CaMnO}_3)_m$ superlattice will also not generate a giant magnetoelectric effect as an applied electric field will not alter much the total amount of charge in LMO or CMO; this is because charge leaked by LMO to CMO on one side is replaced by CMO on the other side.

Based on the above arguments, it should be clear that, compared to experiments involving superlattices where alloy/bulk effect vanishes when the thinner side

of the repeating unit has more than two layers, in our heterostructure bulk nature should vanish when the thinner side has more than 1 layer. Thus, in the superlattice $(\text{LaMnO}_3)_{2n}/(\text{SrMnO}_3)_n$ studied in Ref. 22, the metallic behavior (corresponding to bulk $\text{La}_{0.67}\text{Sr}_{0.33}\text{MnO}_3$) disappears for $n > 2$ and is replaced by insulating behavior; whereas, in the heterostructure $(\text{Ins.})/(\text{LaMnO}_3)_{2n}/\text{Int.}/(\text{SrMnO}_3)_n/(\text{Ins.})$ we expect insulating behavior for $n > 1$. This observation supports our assumption that, in our q2D LMO-CMO heterostructures (corresponding to LCMO that has a narrower band width and a stronger electron-phonon coupling compared to LSMO), only a single narrow-width polaronic band is pertinent. Additionally, interfacial roughness (if considered) will further reduce the band width and suppress metallicity.

Lastly, it should also be pointed out that, in a realistic situation, we have electron-electron repulsion (produced by cooperative electron-phonon interaction) and double-exchange generated ferromagnetic coupling extending to next-nearest-neighbor sites⁶¹ leading to a larger magnetic polaron and thus producing a stronger magnetoelectric effect compared to what our calculations reveal.

V. ACKNOWLEDGEMENTS

S. Y. acknowledges discussions with T. V. Ramakrishnan, D. D. Sarma, and K. Pradhan. S. P. acknowledges discussions with S. Nag, R. Ghosh, S. Kadge, N. Swain, S. Mukherjee, and R. Raman. Work at Argonne National Laboratory is supported by the U.S. Department of Energy, Basic Energy Sciences Materials Science and Engineering, under contract no. DE-AC02-06CH11357.

-
- ¹ C. H. Ahn, A. Bhattacharya, M. Di Ventra, J. N. Eckstein, C. Daniel Frisbie, M. E. Gershenson, A. M. Goldman, I. H. Inoue, J. Mannhart, Andrew J. Millis, Alberto F. Morpurgo, Douglas Natelson, and Jean-Marc Triscone, *Rev. Mod. Phys.* **78**, 1185 (2006).
 - ² J. Chakhalian, J. W. Freeland, A. J. Millis, C. Panagopoulos, and J. M. Rondinelli, *Rev. Mod. Phys.* **86**, 1189 (2014).
 - ³ One striking example is the interface of $\text{LaAlO}_3/\text{SrTiO}_3$ system reported in A. Ohtomo and H. Y. Hwang, *Nature* **427**, 423 (2004); N. Reyren, S. Thiel, A. D. Caviglia, L. Fitting-Kourkoutis, G. Hammerl, C. Richter, C. W. Schneider, T. Kopp, A.-S. Rüetschi, D. Jaccard, M. Gabay, D. A. Muller, J.-M. Triscone, and J. Mannhart, *Science* **317**, 1196 (2007); A. Brinkman, M. Huijben, M. van Zalk, J. Huijben, U. Zeitler, J. C. Maan, W. G. van der Wiel, G. Rijnders, D. H. A. Blank, and H. Hilgenkamp, *Nat. Mater.* **6**, 493 (2007); D. A. Dikin, M. Mehta, C. W. Bark, C. M. Folkman, C. B. Eom, and V. Chandrasekhar, *Phys. Rev. Lett.* **107**, 056802 (2011); N. C. Bristowe, Emilio Artacho, P. B. Littlewood, *Phys. Rev. B* **80**, 045425 (2009).
 - ⁴ N. C. Bristowe, P. B. Littlewood, Emilio Artacho, *J. Phys.: Condens. Matter* **23**, 081001 (2011).
 - ⁵ J. Mannhart and D. G. Schlom, *Science* **327**, 1607 (2010).
 - ⁶ H. Boschker and J. Mannhart, arXiv:1607.07239v1.
 - ⁷ H. Takagi and H. Y. Hwang, *Science* **327**, 1601 (2010).
 - ⁸ G. Hammerl and N. Spaldin, *Science* **332**, 922 (2011).
 - ⁹ H. Y. Hwang, Y. Iwasa, M. Kawasaki, B. Keimer, N. Nagaosa, and Y. Tokura, *Nat. Mater.* **11**, 103 (2012).
 - ¹⁰ E. Dagotto, *Science* **318**, 1076 (2007).
 - ¹¹ L. W. Martin and R. Ramesh, *Acta Materialia* **60**, 2449 (2012).
 - ¹² For a review see J. P. Velev, S. S. Jaswal and E. Y. Tsymsbal, *Phil. Trans. R. Soc. A* **369**, 3069 (2011).
 - ¹³ D. I. Khomskii, *J. Magn. Magn. Mater.* **306**, 1 (2006).
 - ¹⁴ D. Khomskii, *Phys.* **2**, 20 (2009).
 - ¹⁵ K. F. Wang, J. M. Liu, and Z. F. Ren, *Adv. Phys.* **58**, 321 (2009).
 - ¹⁶ M. Fiebig and N. A. Spaldin, *Eur. Phys. J. B* **71**, 293 (2009).
 - ¹⁷ P. Yu, Y.-H. Chu, and R. Ramesh, *Mater. Today* **15**, 320 (2012).
 - ¹⁸ X. Huang and S. Dong, *Mod. Phys. Lett. B* **28**, 1430010 (2014).
 - ¹⁹ J. M. Rondinelli, M. Stengel, and N. A. Spaldin, *Nat. Nanotechnol.* **3**, 46 (2008).
 - ²⁰ M. K. Niranjana, J. D. Burton, J. P. Velev, S. S. Jaswal, and E. Y. Tsymsbal, *Appl. Phys. Lett.* **95**, 052501 (2009).

- ²¹ J. D. Burton and E. Y. Tsymlal, Phys. Rev. B **80**, 174406 (2009).
- ²² A. Bhattacharya, S. J. May, S. G. E. te Velthuis, M. Warusawithana, X. Zhai, Bin Jiang, J.-M. Zuo, M. R. Fitzsimmons, S. D. Bader, and J. N. Eckstein, Phys. Rev. Lett. **100**, 257203 (2008).
- ²³ S. Smadici, P. Abbamonte, A. Bhattacharya, X. Zhai, B. Jiang, A. Rusydi, J. N. Eckstein, S. D. Bader, and J.-M. Zuo, Phys. Rev. Lett. **99**, 196404 (2007).
- ²⁴ S. J. May, A. B. Shah, S. G. E. te Velthuis, M. R. Fitzsimmons, J. M. Zuo, X. Zhai, J. N. Eckstein, S. D. Bader, and A. Bhattacharya, Phys. Rev. B **77**, 174409 (2008).
- ²⁵ A. Bhattacharya, X. Zhai, M. Warusawithana, J. N. Eckstein, and S. D. Bader, Appl. Phys. Lett. **90**, 222503 (2007).
- ²⁶ C. Adamo, X. Ke, P. Schiffer, A. Soukiassian, M. Warusawithana, L. Maritato, and D. G. Schlom Appl. Phys. Lett. **92**, 112508 (2008).
- ²⁷ T. Koida, M. Lippmaa, T. Fukumura, K. Itaka, Y. Matsumoto, M. Kawasaki, and H. Koinuma, Phys. Rev. B **66**, 144418 (2002).
- ²⁸ H. Yamada, M. Kawasaki, T. Lottermoser, T. Arima, and Y. Tokura, Appl. Phys. Lett. **89**, 052506 (2006).
- ²⁹ E. J. Monkman, C. Adamo, J. A. Mundy, D. E. Shai, J. W. Harter, D. Shen, B. Burganov, D. A. Muller, D. G. Schlom, and K. M. Shen, Nat. Mater. **11**, 855 (2012).
- ³⁰ C. Lin, S. Okamoto, and A. J. Millis, Phys. Rev. B **73**, 041104(R) (2006).
- ³¹ C. Lin and A. J. Millis, Phys. Rev. B **78**, 184405 (2008).
- ³² B. R. K. Nanda and S. Satpathy, Phys. Rev. B **78**, 054427 (2008).
- ³³ S. Dong, R. Yu, S. Yunoki, G. Alvarez, J.-M. Liu, and E. Dagotto, Phys. Rev. B **78**, 201102(R) (2008).
- ³⁴ R. Yu, S. Yunoki, S. Dong, E. Dagotto, Phys. Rev. B **80**, 125115 (2009).
- ³⁵ C. Adamo, C. A. Perroni, V. Cataudella, G. De Filippis, P. Orgiani, and L. Maritato, Phys. Rev. B **79**, 045125 (2009).
- ³⁶ Y. Tokura, Rep. Prog. Phys. **69**, 797 (2006).
- ³⁷ See K.H. Kim, M. Uehara, V. Kiryukhin and S.-W. Cheong, in *Colossal Magnetoresistive Manganites*, edited by T. Chatterji, (Kluwer Academic, Dordrecht, 2004).
- ³⁸ C. Martin, A. Maignan, M. Hervieu, and B. Raveau, Phys. Rev. B **60**, 12191 (1999).
- ³⁹ K. Pradhan and A. P. Kampf, Phys. Rev. B **88**, 115136 (2013); J. Salafranca, M. J. Calderón, and L. Brey, Phys. Rev. B **77**, 014441 (2008); D. Niebieskikwiat, L. E. Hueso, J. A. Borchers, N. D. Mathur, and M. B. Salamon Phys. Rev. Lett. **99**, 247207 (2007).
- ⁴⁰ T. F. Seman, K. H. Ahn, T. Lookman, A. Saxena, A. R. Bishop, and P. B. Littlewood, Phys. Rev. B **86**, 184106 (2012).
- ⁴¹ G. G. Guzmán-Verri, R. T. Brierley, P. B. Littlewood, e-print arXiv:1701.02318.
- ⁴² G. V. Pai, S. R. Hassan, H. R. Krishnamurthy, and T. V. Ramakrishnan, Europhys. Lett. **64**, 696 (2003); T. V. Ramakrishnan, H. R. Krishnamurthy, S. R. Hassan, and G. V. Pai, Phys. Rev. Lett. **92**, 157203 (2004).
- ⁴³ N. N. Kovaleva, Andrzej M. Oleś, A. M. Balbashov, A. Maljuk, D. N. Argyriou, G. Khaliullin, and B. Keimer, Phys. Rev. B **81**, 235130 (2010).
- ⁴⁴ S. Datta, A. Das, and S. Yarlagadda, Phys. Rev. B **71**, 235118 (2005).
- ⁴⁵ S. Reja, S. Yarlagadda, and P. B. Littlewood, Phys. Rev. B **84**, 085127 (2011).
- ⁴⁶ R. Pankaj and S. Yarlagadda, Phys. Rev. B **86**, 035453 (2012).
- ⁴⁷ K. Hirota, N. Kaneko, A. Nishizawa, and Y. Endoh, J. Phys. Soc. Jpn. **65**, 3736 (1996); F. Moussa, M. Hennion, J. Rodríguez-Carvajal, H. Moudden, L. Pinsard, and A. Revcolevschi, Phys. Rev. B **54**, 15149 (1996); G. Biotteau, M. Hennion, F. Moussa, J. Rodríguez-Carvajal, L. Pinsard, A. Revcolevschi, Y. M. Mukovskii, and D. Shulyatev, *ibid.* **64**, 104421 (2001).
- ⁴⁸ P. -G. de Gennes, Phys. Rev. **118**, 141 (1960).
- ⁴⁹ Y. A. Izyumov, Y. N. Skryabin, Phys.-Usp. **44**, 109 (2001).
- ⁵⁰ P. W. Anderson, Phys. Rev. **115**, 2 (1959).
- ⁵¹ S. Okamoto and A. J. Millis, Phys. Rev. B **70**, 075101 (2004).
- ⁵² S. Yunoki, A. Moreo, E. Dagotto, S. Okamoto, S. S. Kancharla, and A. Fujimori, Phys. Rev. B **76**, 064532 (2007).
- ⁵³ The on-site Coulomb energy, due to the interaction between an electron on Mn and the positive charge on La, does involve some screening effects due to the oxygen ions surrounding Mn in the perovskite LaMnO₃; in fact, the normal modes such as the Jahn-Teller distortions produce screening. Consequently, $V_s \propto -\alpha$ where $V_s/(-\alpha)$ depends on the effective confining radius and the effective dielectric constant. $V_s/(-\alpha)$ could vary between 3 (for $\epsilon = 20$) and 12 (for $\epsilon = 5$ producing weak screening) when confining radius is $a/3$.
- ⁵⁴ As regards the effective value of the Hubbard U, we know that the occupancy in the d-bands is very largely screened locally either by the change of occupancy in the s-bands (in a metal), or by the oxygen ligands⁵⁵. So while the d-occupancy can change substantially, the actual charge on the positive ion does not. This is what allows the low energies of polaron physics to be relevant in manganites. In an effective one or two band model, all of this screening is subsumed into the interactions⁵⁶.
- ⁵⁵ C. Herring, in *Magnetism*, edited by G. T. Rado and H. Suhl (Academic, New York, 1966), Vol. IV.
- ⁵⁶ W.-G. Yin, D. Volja, and W. Ku, Phys. Rev. Lett. **96**, 116405 (2006).
- ⁵⁷ Z. Zhong and P. Hansmann, Phys. Rev. X **7**, 011023 (2017).
- ⁵⁸ For electrons to flow from LaMnO₃ to CaMnO₃, we only need the work function (WF) of LaMnO₃ to be smaller than the WF of CaMnO₃, i.e., the actual values of the WFs of LaMnO₃ and CaMnO₃ are not relevant for charge transfer.
- ⁵⁹ T. Wu, S. B. Ogale, J. E. Garrison, B. Nagaraj, A. Biswas, Z. Chen, R. L. Greene, R. Ramesh, T. Venkatesan, and A. J. Millis, Phys. Rev. Lett. **86**, 5998 (2001).
- ⁶⁰ Regarding the charge discontinuities at an interface, the polarization (\vec{P}) discontinuity between the LMO side and the CMO side is fixed topologically. Overall difference across the interface does not depend on diffusion of cations near the interface provided the length of diffusion is much smaller than the thickness of the heterostructure and as long as total atoms are conserved. This charge discontinuity is unscreenable in total; the discontinuity produces electric fields (since $\nabla \cdot \vec{P} \neq 0$), though whether or not it is best modeled by a sudden drop from 1 to 0 or an intermediate roll-off (via fractional charges) is a matter of getting detailed atomic relaxations right. The most important point is not the detailed arrangement of charge at the interface, but the total effective charge across the interface (producing polarization discontinuity), which as said

above, is topological (see Ref. 4 for details); for our situation the polarization discontinuity is small.

⁶¹ R. Pankaj and S. Yarlagadda, arXiv:1608.06055.